

Modelling the rate-sensitive characteristics of the Gloucester foundation soil

Sean D. Hinchberger and R. Kerry Rowe

Abstract: Stages 1 (1967) and 2 (1982) of the Gloucester test embankment are studied using a fully coupled finite-element model. The rate-sensitive characteristics of the foundation soil are modelled using an elastoviscoplastic constitutive equation based on the elliptical cap yield surface and Perzyna's overstress theory of viscoplasticity. The aspect ratio of the yield surface for the Gloucester foundation soil is estimated using conventional laboratory shear and consolidation test results. Calculated and measured behaviour during consolidated isotropically undrained triaxial tests and long-term Rowe cell consolidation tests are compared and the ability of the model to describe the measured behaviour of stages 1 and 2 of the Gloucester test embankment is studied. This paper explores the implications of modelling the residual or restructured properties of the Gloucester foundation soil and demonstrates the ability of a single elastoviscoplastic yield-surface model to describe the undrained and drained response of the Gloucester foundation soil during laboratory and field loading conditions.

Key words: elliptical cap, rate sensitive, elastoviscoplasticity, embankment settlements, pore pressures, field performance.

Résumé : Les étapes 1 (1967) et 2 (1982) du remblai d'essai de Gloucester sont étudiées au moyen d'un modèle d'éléments finis complètement couplés. Les caractéristiques de sensibilité à la vitesse de déformation du sol de fondation sont modélisées en utilisant une loi de comportement élasto-viscoplastique basée sur la surface de limite élastique ellipsoïde et la théorie de viscoplasticité en surcontrainte de Perzyna. Le rapport de l'allure de la surface limite pour le sol de fondation de Gloucester est estimé au moyen de résultats d'essais conventionnels de cisaillement et de consolidation en laboratoire. L'on compare les comportements calculé et mesuré au cours des essais triaxiaux consolidés dans des conditions isotropes et non drainées (CIU) et des essais de consolidation à long terme dans la cellule de Rowe, et l'on étudie l'habileté du modèle à décrire le comportement mesuré des étapes 1 et 2 du remblai d'essai de Gloucester. Cet article explore les implications de la modélisation des propriétés résiduelles et restructurées du sol de fondation de Gloucester et démontre l'habileté d'un simple modèle de surface limite élasto-viscoplastique pour décrire la réaction non drainée et drainée du sol de fondation de Gloucester dans des conditions de chargement en laboratoire et sur le terrain.

Mots clés : surface limite ellipsoïde, sensibilité à la vitesse de déformation, élasto-viscoplastique, tassements de remblais, pressions interstitielles, performance sur le terrain.

[Traduit par la Rédaction]

Introduction

The prediction of excess pore pressures, undrained deformations, and long-term settlements of embankments constructed on soft cohesive soil deposits can be difficult when embankment loads cause significant yielding within the foundation soil (e.g., Bozozuk and Leonards 1972; Massachusetts Institute of Technology 1975). Nonlinear elastoplastic yield-surface models (e.g., Roscoe and Schofield 1963; Roscoe and Burland 1968; Chen 1982) have enabled researchers to achieve considerable success in predicting embankment behaviour (e.g., McCarron and Chen 1987); however, as illustrated by Rowe et al. (1996), for some soils these elastoplastic models are not sufficient to ac-

curately model embankment behaviour since, they do not consider soil rheology and consequent rate effects. Rheology models such as the Gibson and Lo model (1961) enable engineers to predict rates of secondary compression (Lo et al. 1976), and Redman and Poulos (1984) showed that a viscoelastic-plastic model could describe undrained creep during short-term embankment loads. There is, however, an apparent need to have an integrated approach to predicting embankment performance which allows for the consideration of yielding, rate effects, consolidation, and creep and to test this formulation against field behaviour.

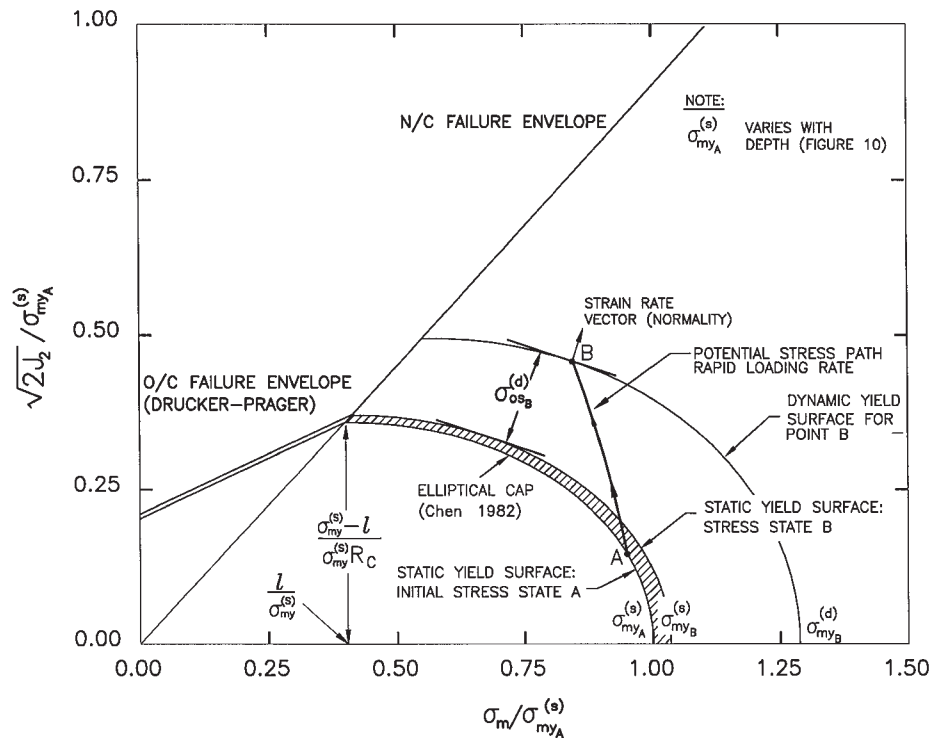
The performance of stage 1 of the Gloucester test embankment (constructed in 1967) has been well documented in the literature (e.g., Bozozuk and Leonards 1972), and several researchers have investigated the behaviour of the Gloucester foundation soil in undrained and drained laboratory tests (e.g., Law 1974; Lo et al. 1976; Leroueil et al. 1983). In June 1982, the second stage of construction for the Gloucester test fill was commenced and the measured response was the subject of a Workshop on the Prediction of the Engineering Behaviour of the Second Stage of the Gloucester

Received September 13, 1996. Accepted June 12, 1998.

S.D. Hinchberger. Acres International Ltd., Niagara Falls, ON L2E 6W1, Canada.

R.K. Rowe. Department of Civil and Environmental Engineering, The University of Western Ontario, London, ON N6A 5B9, Canada.

Fig. 1. Overstress measurement and geometry of elliptical yield surface. N/C, normally consolidated; O/C, overconsolidated.



Test Fill in 1986. Fisher et al. (1982) successfully made a class A prediction of the behaviour of stage 2 of the Gloucester test embankment; however, the method of analysis used for the prediction incorporated a great deal of engineering judgement.

This present paper has three objectives: (i) to study the ability of an elastoviscoplastic yield-surface model to describe the behaviour of the Gloucester foundation soil during long-term Rowe cell oedometer tests, and during consolidated isotropically undrained (CIU) triaxial constant rate of strain compression tests; (ii) to study the ability of an elastoviscoplastic yield-surface model to describe the undrained and drained response of stages 1 and 2 of the Gloucester test embankment; and (iii) to explore the implications of modelling the residual or restructured properties of the Gloucester foundation soil. A new and important aspect of this paper is the demonstrated ability to describe the drained and undrained response of the Gloucester foundation soil during both field and laboratory loading conditions with a single constitutive model.

Elastoviscoplastic elliptical cap model

A detailed subsurface profile for the Gloucester foundation soil has been presented in the literature by Bozozuk and Leonards (1972). In general, the Gloucester foundation soil is a very soft to firm intermediate- to high-plasticity silty clay. In this paper, the rate-sensitive characteristics of the Gloucester foundation soil were modelled using Perzyna's (1963) theory of elastoviscoplasticity wherein the yield function of classical plasticity is coupled with a time-rate rule.

The theoretical formulation adopted is summarized in the Appendix and the basic concepts are illustrated in Fig. 1. An

elliptical cap yield function (Chen 1982) was used to define yielding in the normally consolidated range. If $\sigma_{my}^{(s)}$ is the yield-surface intercept with the mean effective stress, σ'_m , axis ($\sigma'_m = (\sigma'_1 + \sigma'_2 + \sigma'_3)/3$), the elliptical cap is described by the location of the centre of the ellipse at $\sigma'_m = l$ (see Fig. 1), the yield-surface intercept, $\sigma_{my}^{(s)}$, and the yield-surface aspect ratio, R_c , in $(2J_2)^{1/2} - \sigma'_m$ space, where $J_2 = 1/6[(\sigma_{11} - \sigma_{22})^2 + (\sigma_{11} - \sigma_{33})^2 + (\sigma_{22} - \sigma_{33})^2] + (\sigma_{12})^2 + (\sigma_{23})^2 + (\sigma_{31})^2$ is the second invariant of the stress tensor. The expansion of the yield surface is a time-dependent process which is related to the viscoplastic volumetric strain that occurs during a time increment (see eq. [A7] in the Appendix). By definition, the static yield surface defined by $\sigma_{my}^{(s)}$ corresponds to the locus of yield stresses for infinitely slow loading of the soil. For a normally consolidated soil, any load that is not applied infinitely slow may cause the stress state in the soil to change from the initial stress state, such as point A in Fig. 1, to another stress state on the dynamic yield surface (e.g., point B in Fig. 1). The dynamic yield surface is defined by $\sigma_{my}^{(d)}$ as shown in Fig. 1. This point (point B) is assumed to be overstressed relative to the static yield surface by an amount $\sigma_{os}^{(d)}$, which is measured in $(2J)^{1/2} - \sigma'_m$ stress space, and the dynamic yield surface is used to define the potential resultant of the viscoplastic strain-rate vector. While a state of overstress exists, the soil will undergo viscoplastic straining and consequent time-dependent deformation which is proportional to the amount of overstress, $\sigma_{os}^{(d)}$, relative to the static or long-term yield curve. Given sufficient time, the full plastic strains associated with conventional plasticity theory will be achieved.

The theoretical basis for elastoviscoplastic constitutive models has been described extensively in the literature (e.g., Adachi and Okano 1974; Adachi and Oka 1982; Katona

1984; Kavazanjian et al. 1985; Oka et al. 1986; Desai and Zhang 1987). Only basic concepts with respect to the constitutive model used are provided above to allow for more complete comparison of calculated and measured soil behaviour. The elastoviscoplastic elliptical cap model used in this paper most closely resembles the constitutive models of Adachi and Oka (1982) and Katona (1984). However, in the present formulation, an elliptical yield surface (Chen 1982) has been used to define the stress states at yield rather than the Original Cam-Clay yield surface adopted by Adachi and Oka (1982). This modification was introduced to accommodate the fact that the yield surface of clayey soils tends to vary from soil to soil (see Mitchell 1970; Tavenas and Leroueil 1977; Lew 1981; Folkes and Crooks 1985). The aspect ratio of the elliptical yield surface can be changed to account for this variability. An elliptical yield surface was also used by Katona (1984), but the viscoplastic flow rule adopted for the present formulation (see eq. [A6]) is closer to the flow rule proposed by Adachi and Oka (1982) than that adopted by Katona. For the present formulation, the flow rule of Adachi and Oka was modified to better suit the elliptical yield surface based on laboratory studies of the yielding behaviour of natural soils (Hinchberger 1996).

The elliptical cap elastoviscoplastic model described in the Appendix was coupled with Biot consolidation theory and incorporated into the finite-element program AFENA originally developed by Carter and Balaam (1990) and subsequently modified by the authors to allow modelling of elastoviscoplastic behaviour. Details of the finite-element implementation are summarized in the Appendix and are described in more detail by Hinchberger (1996). In addition, Rowe and Hinchberger (1998) have demonstrated the ability of the elastoviscoplastic constitutive model to describe the rate-sensitive behaviour of the Sackville foundation soil.

Laboratory behaviour of Gloucester foundation soil

One-dimensional consolidation

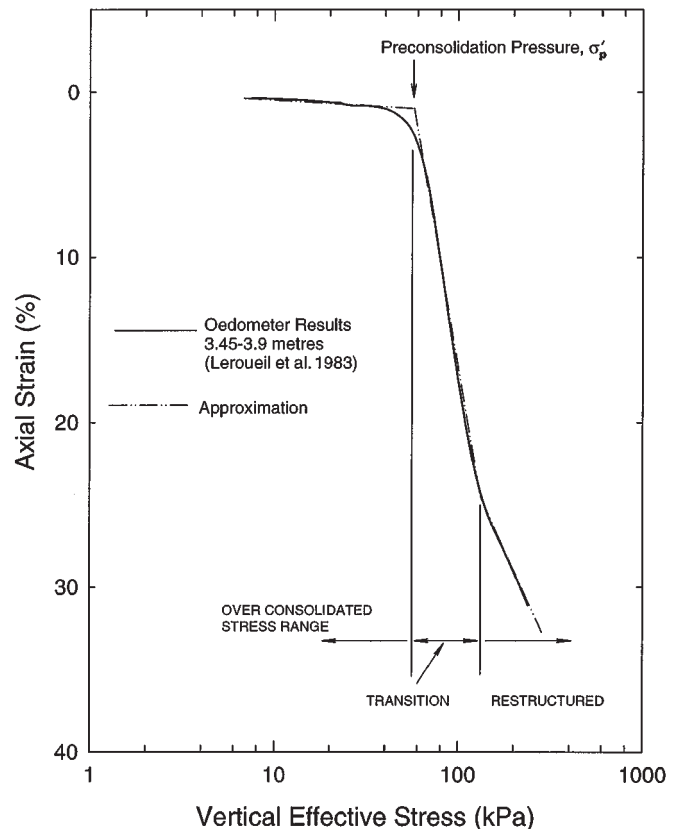
Figure 2 shows a typical consolidation curve for the Gloucester foundation soil. The Gloucester foundation soil has an overconsolidated range and a relatively well defined preconsolidation pressure that is dependent on strain rate during testing (Leroueil et al. 1983). The normally consolidated range may be divided into two distinct phases as suggested by Silvestri (1984a) and shown in Fig. 2. The first phase is a transitional phase where the natural cemented structure of the Leda Clay is broken down. The second phase is the restructured phase. For the purpose of modelling the deformation characteristics of the Gloucester foundation soil the normally consolidated phase was considered to be bilinear (see Fig. 2). This will be discussed further when comparing the calculated and measured behaviour of stage 2 of the Gloucester test embankment.

Behaviour during long-term Rowe cell consolidation

Selection of material properties

Lo et al. (1976) published the results of long-term Rowe cell consolidation tests for Gloucester foundation soil from depths of 2.4 and 4.2 m, respectively (see Fig. 3). These

Fig. 2. Typical oedometer consolidation behaviour of Gloucester foundation soil. Bilinear approximation in normally consolidated stress range.

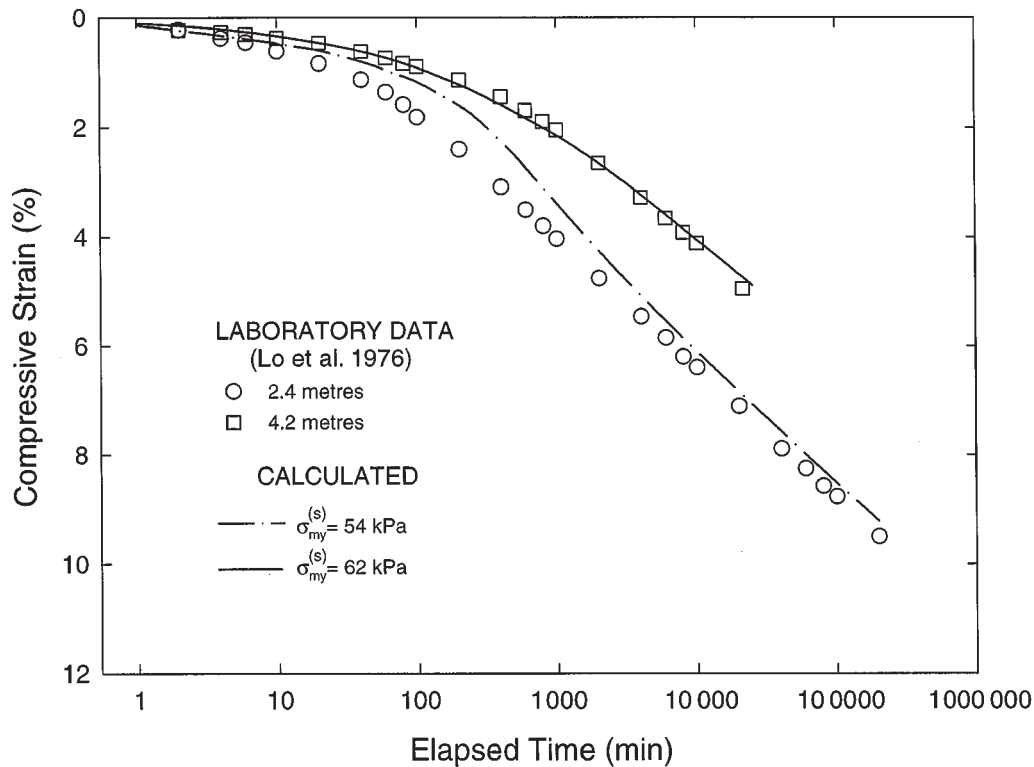


tests were modelled using the elastoviscoplastic model (see Appendix) by discretizing the soil sample using cubic strain triangles and assuming axisymmetric conditions.

The hydraulic conductivity, k , of the Gloucester foundation soil was considered to be dependent on the void ratio as follows:

$$[1] \quad k = k_0 \exp\left(\frac{e - e_0}{C_k}\right)$$

where e_0 is the reference void ratio, k_0 is the hydraulic conductivity at the reference void ratio, e is the void ratio, and C_k is the slope of the $e - \log(k)$ plot. Equation [1] was also used by Mesri and Choi (1979) to describe the change in hydraulic conductivity with void ratio for the Gloucester foundation soil using $C_k = 1.0$. A value of $C_k = 0.25$ estimated from the results of hydraulic conductivity tests at depths of 2.13, 2.74, and 3.96 m (summarized in Table 1) was adopted in this paper. The hydraulic conductivity test results listed in Table 1 were obtained at the National Research Council of Canada (NRC). The value of C_k was found to be highly variable below 5.2 m; however, the hydraulic conductivity tests at 2.13, 3.74, and 3.96 m are more applicable to the long-term laboratory consolidation tests on soil from a depth of 4.2 m. In addition to $C_k = 0.25$, $k_0 = 2.5 \times 10^{-9}$ m/s was selected for both test simulations so that the calculated time to 90% dissipation of excess pore pressures was 350 min as reported by Lo et al. (1976). This initial hydraulic conductiv-

Fig. 3. Comparison of calculated and measured compressive strains during long-term Rowe cell oedometer tests.**Table 1.** Hydraulic conductivity test results at initial and final in situ stresses for stage 1 of the Gloucester test embankment (data supplied by NRC).

Depth (m)	Initial			Final			C_k
	Water content w (%)	Void ratio e	Hydraulic conductivity k ($\times 10^9$ m/s)	Water content w (%)	Void ratio e	Hydraulic conductivity k ($\times 10^9$ m/s)	
2.13	88.5	2.39	2.7	76.4	2.06	0.9	0.30
2.74	74.7	2.02	2.0	62.6	1.69	0.4	0.21
3.96	85.4	2.31	2.0	66.5	1.80	0.1	0.19
5.18	64.4	1.74	1.1	61.5	1.66	0.9	0.54
5.64	59.0	1.59	0.6	56.8	1.53	0.6	0.54
7.38	101.6	2.74	2.5	97.8	2.64	1.8	0.29
8.53	94.0	2.54	1.4	91.3	2.47	1.3	1.11
10.36	94.2	2.54	1.6	91.9	2.48	0.9	0.11
12.19	82.8	2.23	1.2	82.1	2.21	0.9	0.07
13.41	47.2	1.27	1.6	46.0	1.24	1.3	0.15
15.24	56.7	1.53	1.4	55.7	1.50	0.8	0.06
17.68	64.3	1.74	1.8	62.7	1.69	1.7	0.73
20.73	30.6	0.82	2.7	29.6	0.80	2.7	0.0

Note: Hydraulic conductivity k was derived using eq. [1], and C_k is the slope of the $e - \log(k)$ plot.

ity also compares favourably with the results of hydraulic conductivity tests (see Table 1) for soil from these depths.

The recompression index, κ , was estimated to be 0.025 for the Gloucester foundation soil based on consolidation curves published by Leroueil et al. (1983). The compression index, λ , was selected to be 0.65 based on the results of conventional oedometer consolidation tests on soil from comparable depths (see Fig. 4). The slope of the failure envelope ($(2J_2)^{1/2} - \sigma_m'$ stress space) in the normally consolidated stress range was taken to be $M = 0.9$, with a cohesion inter-

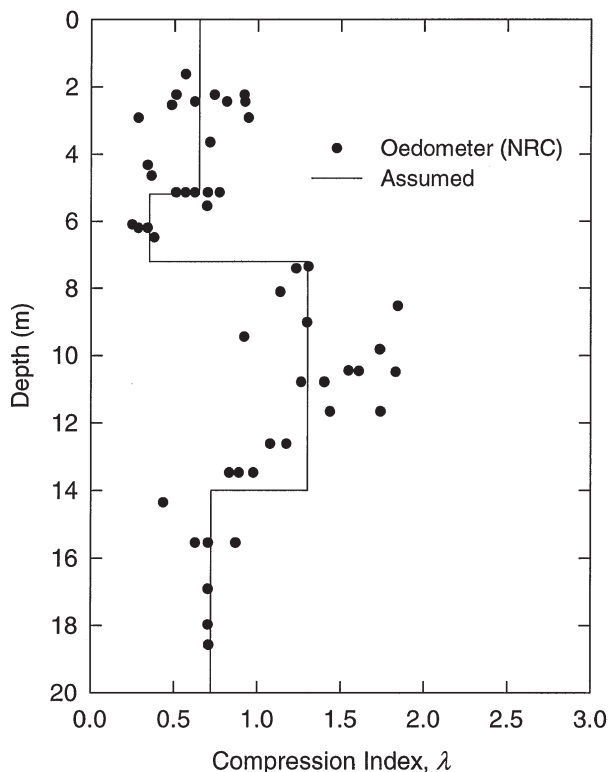
cept of $c'_k = 0$ based on the failure envelope obtained by Law (1974) for the Gloucester foundation soil. The aspect ratio, $R_c = 1.65$, of the elliptical yield surface was selected on the basis of both long-term consolidation tests and CIU triaxial tests which will be discussed in more detail in a later section. Table 2 contains a list of all material constants used to calculate the long-term Rowe cell consolidation behaviour of the Gloucester foundation soil, and Table 3 summarizes the stress increments used by Lo et al. (1976) and sample information.

Table 2. Assumed material properties for long-term Rowe cell consolidation simulations.

Poisson's ratio, ν	0.3
Viscoplastic fluidity constant, γ^{vp} (s^{-1})	1.67×10^{-10}
Strain-rate exponent, n	30.0
Reference or initial void ratio, e_0	1.8
Hydraulic conductivity at reference void ratio, k_0 (m/s)	2.5×10^{-9}
Slope of $e - \log(k)$ plot, C_k	0.25
Recompression index based on $e - \ln \sigma$ curve, κ	0.025
Compression index based on $e - \ln \sigma$ curve, λ	0.65

Table 3. Sample information and stress increments for Rowe cell consolidation tests.

Sample type	Sample size (mm)	Depth (m)	Natural moisture content, w_n (%)	Preconsolidation pressure, σ_p' (kPa)	Stress increment (kPa)
Block	150 × 50	2.4	66.1	62.0	42.9–90.0
Osterberg	112.5 × 50	4.2	70.6	69.0	48.2–92.3

Fig. 4. Compression index, λ , versus depth. Data supplied by the National Research Council of Canada (NRC).

Comparison of calculated and experimental behaviour

Figure 3 illustrates the general ability of the elastoviscoplastic elliptical cap model (with $R_c = 1.65$) to describe the secondary compression behaviour of the Gloucester soil during long-term Rowe cell consolidation tests. At a depth of 2.4 m, the elliptical cap constitutive model predicted more delayed compression in the early stages of the long-term Rowe cell consolidation test than that of the measured response. This difference in the early stages of the test is small and may be the result of differences between the assumed and actual yield-surface shape for the Gloucester soil, and the calculated and actual stress path during the test. There is better agreement between calculated and measured behav-

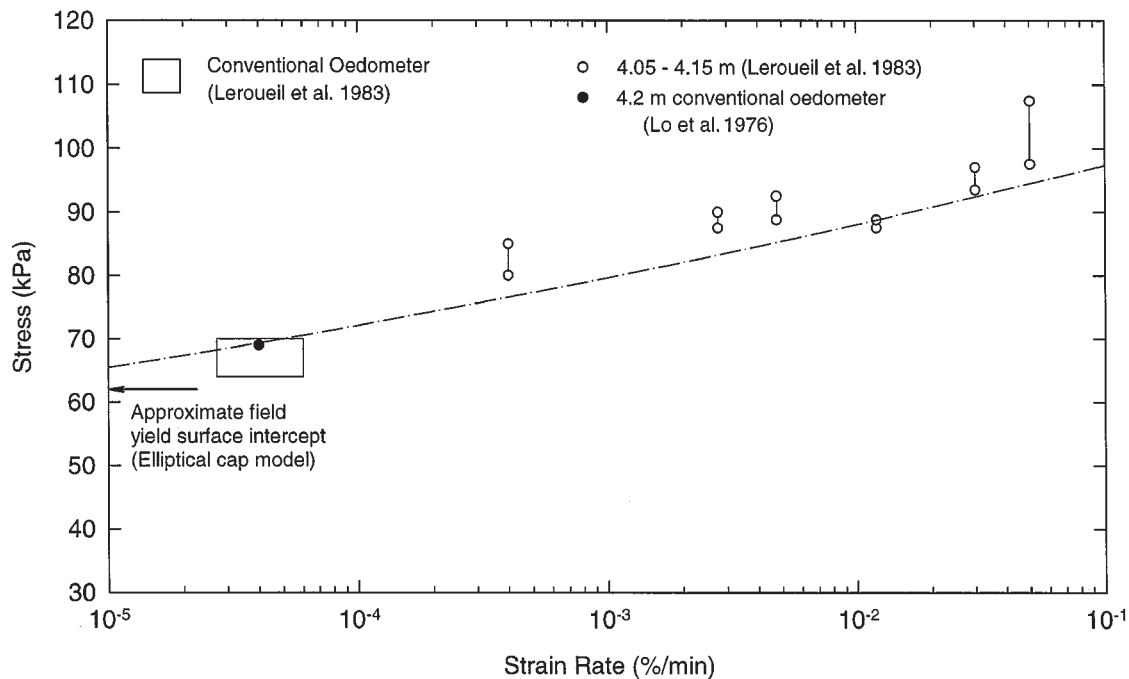
our for soil from a depth of 4.2 m, indicating that the difference between calculated and measured behaviour for soil from 2.4 m may also be the result of soil variability.

The yield-surface intercepts, $\sigma_{my}^{(s)}$, which resulted in the best fit to the measured behaviour were 54 kPa for soil from 2.4 m and 62 kPa for soil from 4.2 m. A fluidity constant, γ^{vp} , of $1.67 \times 10^{-10} s^{-1}$ was inferred for soil from both depths based on the fit of Rowe cell consolidation test data and CIU triaxial shear test results that will be discussed in a later section. The strain-rate parameter, n , was selected so that the calculated rates of secondary compression matched the measured rates (n is inversely proportional to the rate of secondary compression). Furthermore, the yield-surface intercepts of 54 and 62 kPa are less than the preconsolidation pressures of 62 and 69 kPa reported by Lo et al. (1976) for conventional oedometer consolidation on soil from 2.4 and 4.2 m, respectively. This is consistent with the concepts of overstress viscoplasticity, since the field preconsolidation pressures generally correspond to infinitesimal or very slow strain rates, whereas laboratory preconsolidation pressures are typically measured at higher strain rates.

Leroueil et al. (1983) established that the measured preconsolidation pressure of the Gloucester foundation soil was strain-rate dependent, and the results published by both Lo et al. (1976) and Leroueil et al. (1983) show that rate effects are less significant for stress states below yield. For stress states that exceed yield, the behaviour of the Gloucester foundation soil during long-term consolidation tests was found to be dominated by secondary compression (Lo et al. 1976). Furthermore, the yield pressure of the Gloucester foundation soil was found to be strongly influenced by strain rate (Leroueil et al. 1983). This provides some justification for the use of elastoviscoplastic theory to describe the behaviour of the Gloucester soil.

The analysis of long-term Rowe cell consolidation tests using the elliptical cap elastoviscoplastic constitutive model suggests that the field yield-surface intercept of the Gloucester foundation soil is marginally less than the preconsolidation pressure measured during conventional oedometer consolidation. On average, the preconsolidation pressure obtained from conventional incremental oedometer consolidation tests was found to be approximately 14% greater than the static yield-surface intercept back-calculated using the elliptical

Fig. 5. A comparison of the preconsolidation pressures measured by Leroueil et al. (1983) and Lo et al. (1976) with the field (static) yield-surface intercept for the Gloucester foundation soil.



cap elastoviscoplastic model with $R_c = 1.65$. Figure 5 shows the apparent preconsolidation pressure versus strain rate measured by Leroueil et al. (1983) for soil from a depth of 4.05–4.15 m. Also included in Fig. 5 is the preconsolidation pressure reported by Lo et al. (1976) for soil from a depth of 4.2 m which lies within the range of preconsolidation pressures obtained by Leroueil et al. (1983) for incremental oedometer consolidation. The strain-rate dependency of the Gloucester foundation soil during laboratory consolidation tests is evident in Fig. 5 and the position of the field yield-surface intercept for the elliptical cap constitutive model ($R_c = 1.65$) is also indicated in Fig. 5. Silvestri (1984b) showed that a simple power law (Norton 1929) could be used to correct preconsolidation pressures measured at higher strain rates during constant gradient and constant rate of strain consolidation tests back to the preconsolidation pressures obtained from conventional oedometer consolidation at lower strain rates. Figure 5 suggests that preconsolidation pressures obtained during incremental oedometer consolidation may also require a correction for the difference between laboratory strain rates and field strain rates.

The foregoing discussion and comparisons provide some basis for using the elliptical cap elastoviscoplastic constitutive equation to model the long-term behaviour of the Gloucester test embankment. The model can adequately describe the secondary compression behaviour of the Gloucester foundation soil during long-term Rowe cell consolidation tests. Recognizing that the elliptical cap elastoviscoplastic constitutive model implies the presence of a field preconsolidation pressure that is marginally lower than the preconsolidation pressure measured during incremental oedometer consolidation, a factor of 1/1.14 will be applied

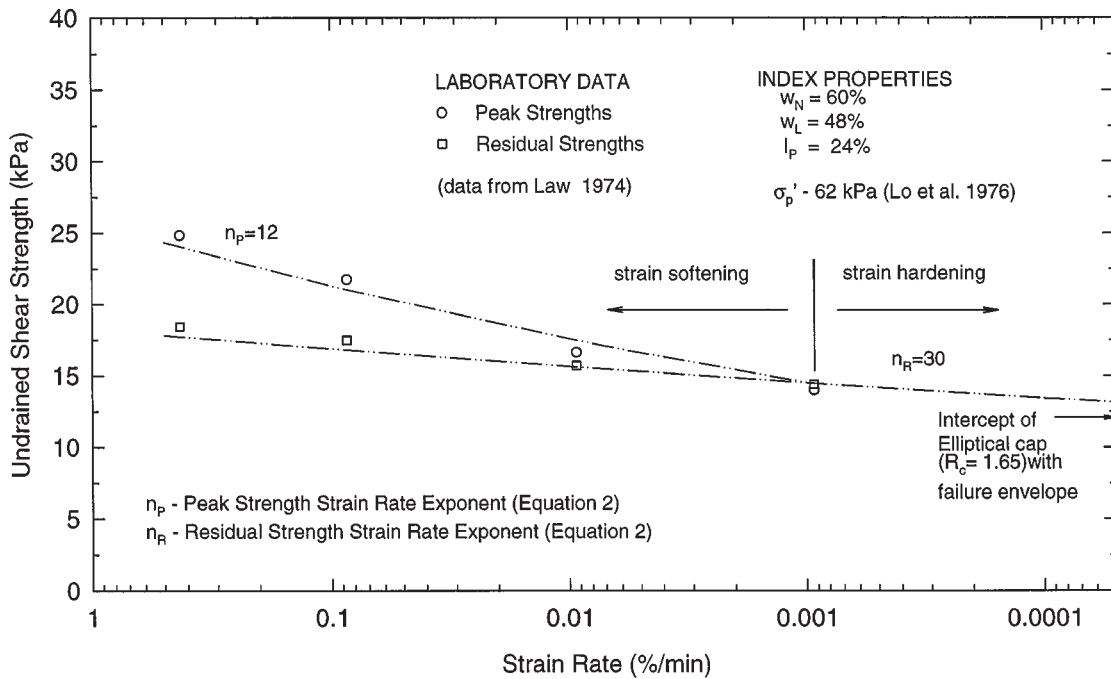
to the laboratory oedometer preconsolidation pressure to estimate the field yield-surface intercept. It is now necessary to justify the use of an aspect ratio, R_c , of 1.65 for the elliptical cap model.

Behaviour during undrained triaxial shear

Strain-rate behaviour during undrained unconsolidated triaxial shear

Figure 6 shows the measured peak and postpeak strengths of the Gloucester foundation soil during unconsolidated undrained (UU) triaxial tests at different strain rates (Law 1974). The figure illustrates two important properties of the Gloucester soil, namely (i) the dependency of both the peak and postpeak strength on the axial strain rate, and (ii) the transition from a strain-softening to a strain-hardening behaviour as the axial strain rate is reduced. The increased shear strength with increased strain rate illustrates the concept of overstress viscoplasticity. As the strain rate increases, the amount of overstress above the long-term (static) shear strength increases. The shear strength of the Gloucester foundation soil decreases with diminishing strain rate to a value of 13 kPa at a strain rate of 0.0001%/min. Stage 1 of the Gloucester test embankment was constructed to a height of 2.4 m above the original ground level during a 10 day period (Bozozuk and Leonards 1972). Leroueil et al. (1983) estimated from field data that the in situ strain rate within the foundation soil at the end of construction was approximately 2×10^{-5} %/min, and about 2×10^{-6} %/min at 1.5 years after the end of construction. The low in situ strain rates combined with Fig. 6 make it reasonable to assume that the strain-hardening range of behaviour is operative in the field during construction of the Gloucester test embank-

Fig. 6. The effects of strain rate on the peak and postpeak shear strength of Gloucester foundation soil (Law 1974); constant rate of strain UU triaxial tests. w_N , natural moisture content; w_L , liquid limit; I_p , index of plasticity.



ment. The strain-softening behaviour of the Gloucester foundation soil appears to be strain-rate induced and Gloucester soil from a depth of 2.4 m tends towards the residual state (exhibiting no peak–postpeak response) during UU triaxial tests at axial strain rates less than approximately 0.01%/min. Lo and Morin (1972) found that Leda clay from Saint Vallier and Saint Louis also tended toward the residual or restructured state as strain rates became small during consolidated anisotropically undrained (CAU) and consolidated isotropically drained (CID) triaxial tests.

The intercept of the elliptical yield surface (with $R_c = 1.65$ and $\sigma_{my}^{(s)} = 54$ kPa) with the failure envelope is plotted in Fig. 6. The static yield-surface intercept, $\sigma_{my}^{(s)} = 54$ kPa, was inferred from the long-term Rowe cell consolidation test for soil from a depth of 2.4 m (see Fig. 3). The measured residual undrained shear strengths during UU triaxial tests tend toward the theoretical long-term shear strength corresponding to the intersection of the elliptical cap ($R_c = 1.65$) with the failure envelope. Based on the case records reported by Bozozuk and Leonards (1972), Lo et al. (1976), and Fisher et al. (1982), the range of in situ mean effective stress at a depth of 2.4 m is approximately 20–30 kPa. The elliptical yield surface ($R_c = 1.65$ and $\sigma_{my}^{(s)} = 54$ kPa) intersects the failure envelope at a mean effective stress of 21.7 kPa. Thus it is reasonable to assume that the effective stress path during UU triaxial tests at a depth of 2.4 m will tend toward a stress state at failure which is similar to the intersection of the yield surface with the failure envelope.

Lastly, the measured residual shear strength versus strain rate data in Fig. 6 was also fit with Norton’s (1929) law, viz.,

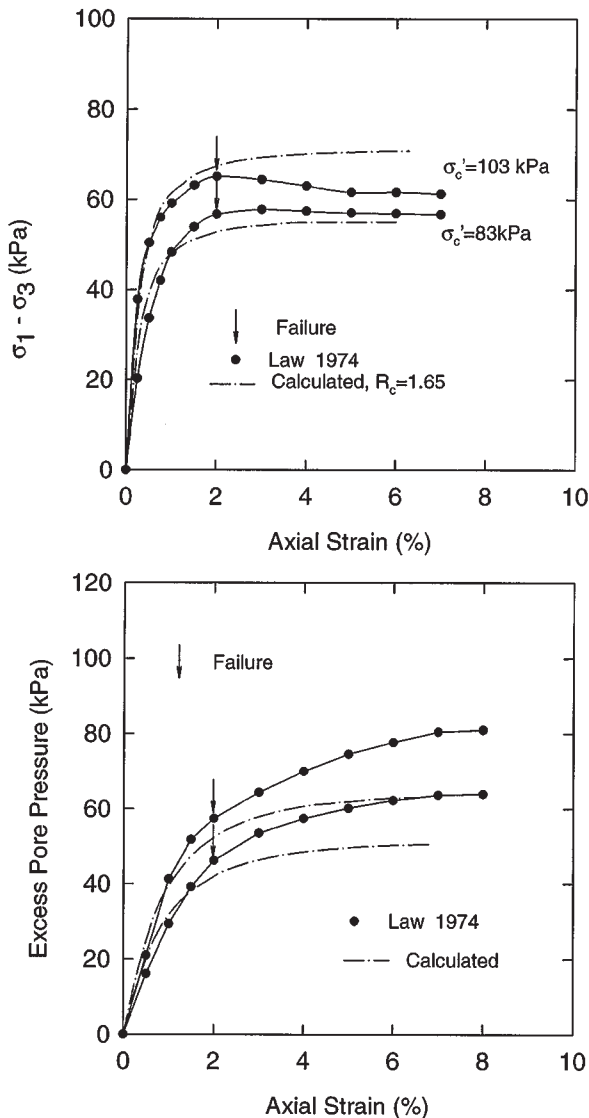
$$[2] \quad \dot{\epsilon}_{11} = \gamma^{vp} \left(\frac{c_u^{(d)}}{c_u^{(s)}} \right)^n$$

where n is the strain-rate exponent (see Fig. 6), $c_u^{(d)}$ is the strain-rate-dependent undrained shear strength, and $c_u^{(s)}$ is the undrained shear strength corresponding to $\dot{\epsilon}_{11} = \gamma^{vp}$. It is important to note that the strain-rate parameter, $n = 30$, required to fit results of the long-term Rowe cell consolidation from a depth of 2.4 m is the same as the strain-rate parameter, $n_R = 30$, obtained using Norton’s law (1929) to fit the residual undrained shear strength versus strain-rate data (see Fig. 6). Hinchberger (1996) showed that eq. [2] may be used to estimate the viscoplastic constants for the elliptical cap elastoviscoplastic constitutive equation using the plot of undrained shear strength versus strain rate.

Behaviour during CIU triaxial shear

Figure 7 shows the comparison between CIU triaxial compression test results for the Gloucester foundation soil from a depth of 2.4 m with the calculated behaviour using elliptical cap viscoplasticity ($R_c = 1.65$). The consolidation phase of the CIU tests was 24 h (Law 1974) and the consolidation pressures exceeded the measured preconsolidation pressure of the Gloucester soil. Compression occurred at an axial strain rate of 0.017%/min. The consolidation phase of the CIU tests was modelled numerically for axisymmetric conditions with radial drainage. The slope of the failure envelope, M , in $(2J)^{1/2} - \sigma'_m$ stress space was taken to be 0.9 with a cohesion of $c'_k = 0$ based on the results of Law (1974). For each CIU triaxial compression test, the initial position of the static yield surface was taken to be 54 kPa based on the results of fitting the long-term Rowe cell consolidation test results for soil from a depth of 2.4 m. The positions of the yield surface, void ratio, and stress state at the end of the 24 h consolidation phase were calculated and then used as initial input parameters for the CIU triaxial test simulations. Modelling the consolidation phase of the CIU triaxial com-

Fig. 7. Comparison of calculated and measured behaviour during CIU triaxial shear.



pression tests using the elliptical cap elastoviscoplastic constitutive equation accounts for the effects of secondary compression and aging on the position of the yield surface at the end of the 24 h consolidation phase.

Referring to Fig. 7, it can be seen that an elliptical cap with an aspect ratio, R_c , of 1.65 adequately describes the behaviour of the Gloucester foundation soil during CIU triaxial compression tests. The calculated axial stress versus axial strain response for tests corresponding to consolidation pressures of 83 and 103 kPa is close to the measured response up to failure. The calculated peak shear strength is approximately 3% below the measured peak shear strength at a cell pressure of 83 kPa and 8% greater than the measured peak shear strength at a cell pressure of 103 kPa.

The theoretical pore pressures are generally close to the measured behaviour up to failure. Failure was defined by Law (1974) to be $(\sigma_1 - \sigma_3)_{\max}$. At failure, the calculated pore pressures peak while the measured pore pressures continued to increase. The increase in pore pressure for strains in ex-

cess of the failure strains (see Fig. 7) cannot be predicted using the elliptical cap viscoplastic model.

Stage 1: Gloucester test embankment

Finite-element discretization

The finite-element mesh used to model stages 1 (1967) and 2 (1982) of the Gloucester test embankment consisted of 800 six-noded linear strain triangles (each with three integration points) and 1702 nodes. Figure 8 shows the geometry and finite-element mesh used to model stages 1 and 2 of the Gloucester test embankment. As previously noted, the detailed subsurface profile may be found in publications by Bozozuk and Leonards (1972), Lo et al. (1976), and Fisher et al. (1982). The foundation soil was modelled as an elastoviscoplastic material coupled with Biot consolidation theory under plane-strain conditions. Based on field data, a rigid permeable boundary condition was assumed at a depth of 20.2 m. The foundation soil was modelled 75 m beyond the embankment centreline, and at this location a smooth rigid permeable boundary was assumed. The interface between the foundation and embankment soils was considered to be purely cohesive and modelled using six-noded zero thickness joint (or slip) elements. The finite-element analysis of the Gloucester test embankment, however, showed that slip at this interface did not occur.

The excavation portion of stage 1 construction was simulated by removing excavated elements from the finite-element mesh and incrementally removing the nodal forces associated with the internal stresses and unit weight of the elements. Similarly, construction of the embankment was simulated by adding rows of elements and incrementally increasing the body forces due to gravity within these elements. The time increments used to march the solution forward in time ranged from 0.25 h during the short-term undrained conditions to 10 h near the end of stage 1 monitoring.

Material properties

Embankment fill

The embankment fill was modelled as an elastoplastic (inviscid) material with a Mohr-Coulomb failure criterion and a flow rule of the form proposed by Davis (1968). Based on the results of Bozozuk and Leonards (1972), the fill material was assumed to be cohesionless with an effective friction angle $\phi' = 35^\circ$, a dilation angle $\psi = 0^\circ$, and a unit weight equal to 18.4 kN/m^3 . The Young's modulus of the fill was assumed to be dependent on the minor principal stress and described using the equation of Janbu (1963), viz.,

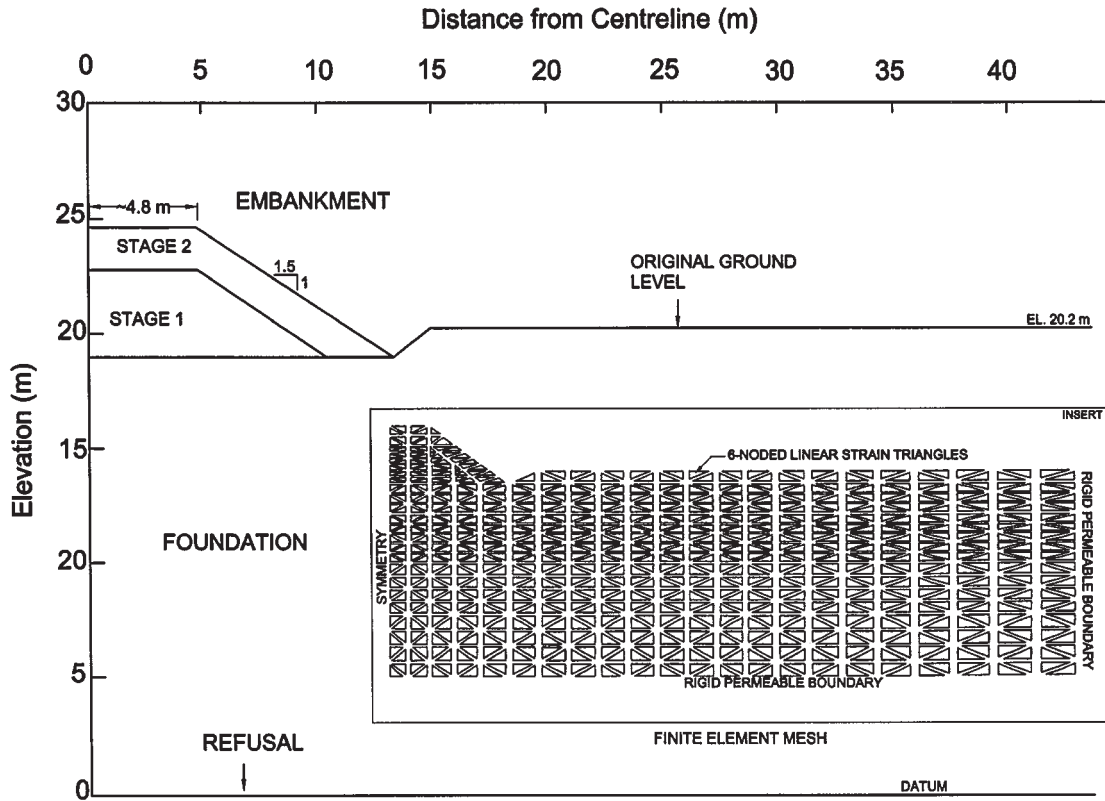
$$[3] \quad \frac{E}{P_a} = K_E \left(\frac{\sigma_3}{P_a} \right)^m$$

where E is the Young's modulus of the soil, P_a is the atmospheric pressure, σ_3 is the minor principal stress, and K_E (250) and m (0.5) are based on Rowe et al. (1984).

Hydraulic conductivity profile

The hydraulic conductivity profile used to obtain the calculated behaviour of the Gloucester test embankment is compared with the measured hydraulic conductivities prior

Fig. 8. Geometry and finite-element mesh for stages 1 and 2 of the Gloucester test embankment.



to construction of stage 1 in Fig. 9. A hydraulic conductivity value that was intermediate to the field and laboratory test measurements was assumed for much of the deposit. Higher conductivities for the upper 4 m of the foundation deposit were investigated, since laboratory tests indicated that the hydraulic conductivity near the foundation surface may be significantly higher than those measured from field tests at greater depths. The results of this investigation showed that the agreement between calculated and measured behaviour was adequate over the range of measured conductivity values. The assumed profile of initial vertical hydraulic conductivity as shown in Fig. 9 was found to provide the best fit to the measured field behaviour.

The decrease in hydraulic conductivity with decreasing void ratio was described using eq. [1] with a value of C_k of 0.25 for the entire deposit, as previously discussed. Although Table 1 shows that the value of C_k is variable for depths below 5.2 m, a constant value of 0.25 was adopted based on the hydraulic conductivity tests that exhibited a significant change in void ratio between the initial and final consolidation pressures. The anisotropic characteristics of the Gloucester foundation soil were modelled and the ratio of horizontal to vertical hydraulic conductivity, k_h/k_v , was taken to be 1.25 based on data supplied by NRC.

Groundwater conditions

Bozozuk and Leonards (1972), among others, suggested that the groundwater table was 1.6 m below the original ground surface. This may have been the case prior to construction and during the early stages of stage 1; however, the available case records indicate that the groundwater table was about 0.4 m below the original ground level during both

Fig. 9. In situ hydraulic conductivity measurements and laboratory hydraulic conductivity results (data supplied by NRC).

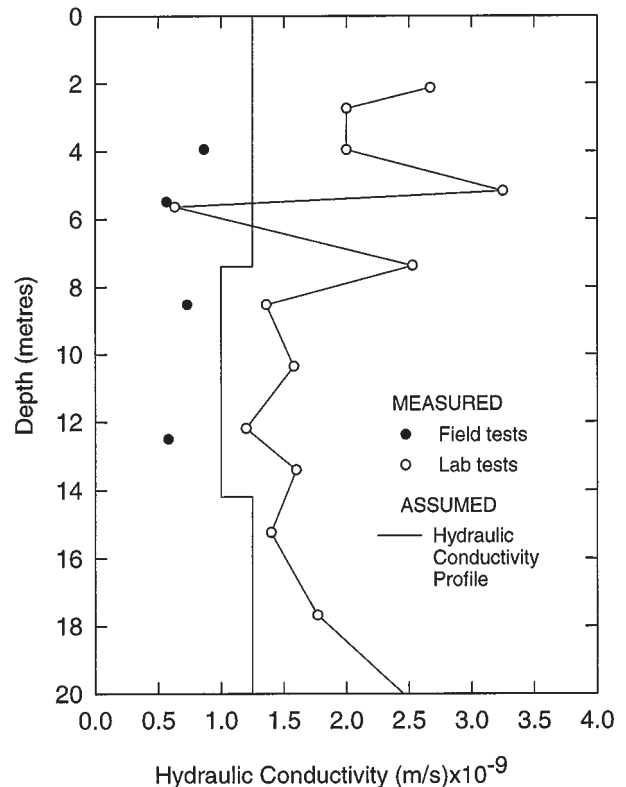


Table 4. Material properties assumed for analysis of the Gloucester test embankment.

Depth (m)	κ	λ	e_o	k_o ($\times 10^{-9}$ m/s)	C_k	k_h/k_v	ν	γ ($\times 10^{-10}$ s $^{-1}$)	n	R_c	M
0.0–2.0	0.025	0.65	1.8	1.2	0.25	1.25	0.3	1.67	30	1.65	0.9
2.0–5.2	0.025	0.65	1.8	1.2	0.25	1.25	0.3	1.67	30	1.65	0.9
5.2–7.2	0.025	0.32	1.8	1.0	0.25	1.25	0.3	1.67	30	1.65	0.9
7.2–13.4	0.025	1.35	2.4	1.0	0.25	1.25	0.3	1.67	30	1.65	0.9
13.4–20.2	0.025	0.72	1.8	1.2	0.25	1.25	0.3	1.67	30	1.65	0.9

Note: k_h , horizontal hydraulic conductivity; k_v , vertical hydraulic conductivity; R_c , yield-surface aspect ratio; M , slope of the failure envelope in $(2J_2)^{1/2}$ - σ_m' stress space. Other symbols as defined in Table 3.

stage 1 and stage 2 of the Gloucester test embankment construction (Fisher et al. 1982), and this assumption was adopted for the present analysis.

Consolidation characteristics

The assumed compression index, λ , profile is plotted in Fig. 4 with the results from incremental oedometer consolidation tests. The assumed profile of λ with depth is essentially an average of the measured values supplied by NRC. The recompression or swelling index, κ , was taken to be 0.025 for the entire deposit. The value of 0.025 was selected based on the consolidation curves published by Leroueil et al. (1983), and a sensitivity study showed that the assumed value of κ had only a small effect on the calculated settlements.

Figure 10 shows the measured preconsolidation pressure profile (laboratory measurements by NRC) and the assumed yield-surface profile for the analysis of the Gloucester test embankment. The oedometer preconsolidation pressures were corrected for strain-rate effects by applying the factor 1/1.14 as discussed previously. Thus, the calculated 14% difference between the measured oedometer preconsolidation pressures and the field static yield-surface intercept for the elliptical cap elastoviscoplastic model is reflected in Fig. 10. Table 4 lists all material constants used in the analysis of stages 1 and 2 of the Gloucester test embankment.

K'_o conditions

The selection of the coefficient of earth pressure at rest K'_o profile was based on the results of hydraulic fracturing tests by Bozozuk (1974). Based on this, the upper 5.2 m of the foundation was assigned a K'_o value of 1.0, and a value of 0.8 was adopted for the remainder of the deposit. A K'_o value of 0.8 for the entire deposit was also investigated and found to have only a small influence on the calculated settlements for stage 1.

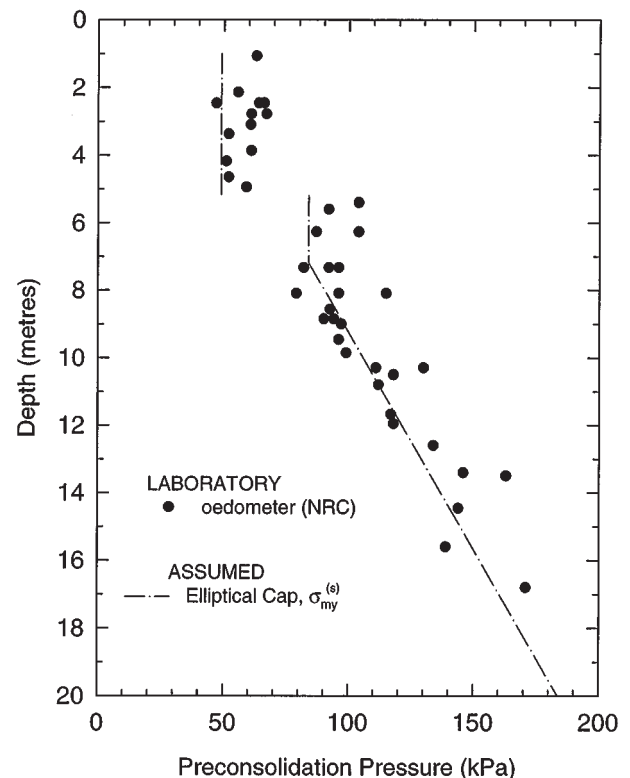
Failure envelope

Based on the research of Law (1974) for Gloucester foundation soil from a depth of 2.4 m (see also Fisher et al. 1982), the slope of the failure envelope in $(2J_2)^{1/2}$ - σ_m' stress space was taken to be $M = 0.9$ ($\equiv \phi' = 25^\circ$) with a cohesion intercept $c'_k = 0$ (see Appendix) for the entire foundation soil deposit.

Calculated behaviour

Settlements

The calculated settlements at gauges S1, S2, S3, and S4 beneath the embankment centreline are compared with the

Fig. 10. Preconsolidation pressure versus depth (data provided by NRC).

measured settlements in Fig. 11, and Fig. 12 shows the same comparison for settlement gauges S6, S7, and S8 beneath the embankment shoulder. Beneath the embankment centreline the calculated settlements compare favourably with the measured settlements. The settlements are slightly overestimated at gauges S1 and S2 and those at gauge S3 are underestimated. This may be attributed to variations in the soil profile. Beneath the embankment shoulder the calculated settlements also compare favourably with the measured settlements. At the location of settlement gauge S6, the calculated settlement 5000 days after the end of construction is 19 cm compared with a measured settlement of approximately 21 cm. Although there are no long-term settlement data available for gauge S7, the initial performance is close to the calculated behaviour. In general, it was found that the elliptical cap elastoviscoplastic constitutive model adequately described the settlement behaviour of stage 1 of the Gloucester test embankment. Fluctuations in the groundwa-

Fig. 11. Predicted and measured displacements at centreline for stage 1 of the Gloucester test embankment. Elliptical cap model ($R_c = 1.65$). S1–S4, settlement gauges.

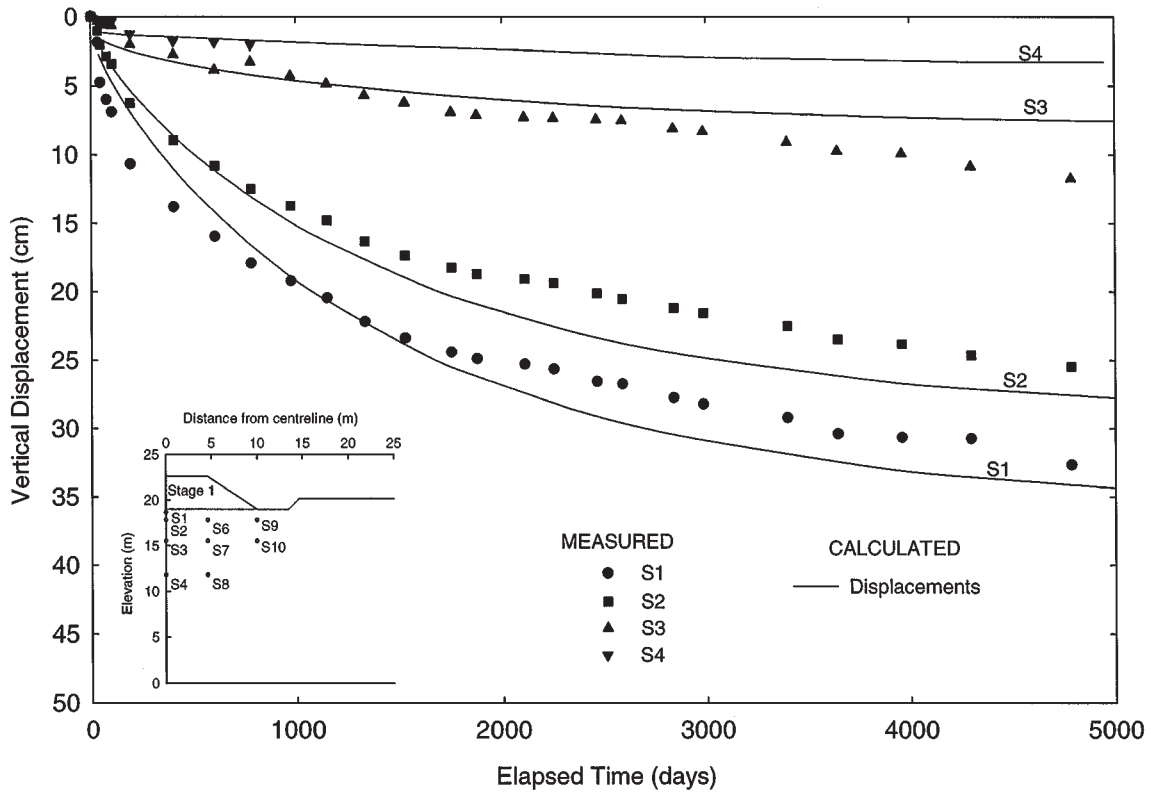


Fig. 12. Predicted and measured displacements beneath shoulder for stage 1 of the Gloucester test embankment. Elliptical cap model. S6–S8, settlement gauges.

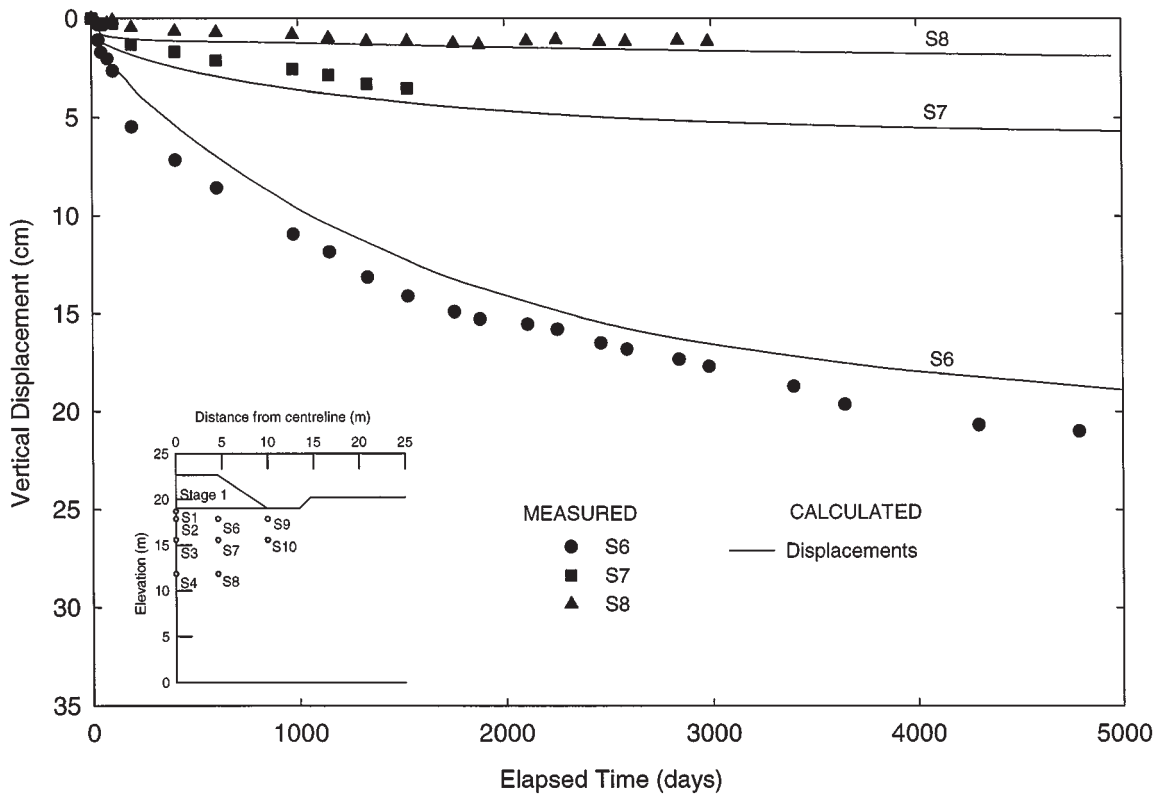
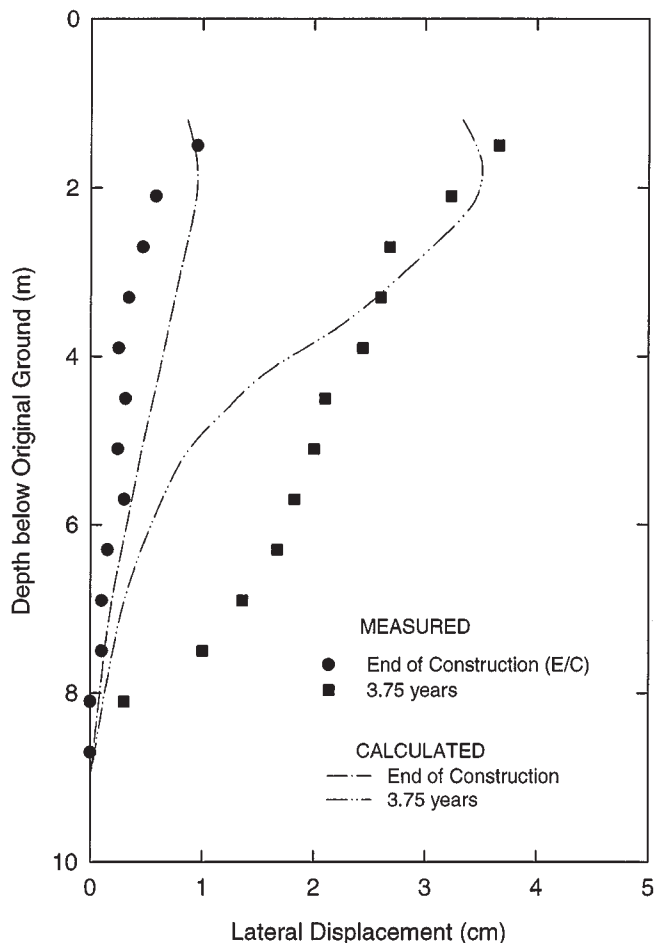


Fig. 13. Lateral displacements at embankment toe for stage 1 of the Gloucester test embankment.



ter conditions and moisture content of the embankment fill during the case history can account for the fluctuations in the field measurements.

Lateral displacements

Figure 13 shows the relative horizontal displacements at the embankment toe at the end of construction and 3.75 years after the end of construction. At the end of construction, the calculated horizontal displacement at the ground surface is approximately 0.95 cm and the measured lateral deformation is approximately 1 cm. The calculated horizontal displacements exceed the measured displacements between 1.7 and 5.8 m below the original ground level, and the agreement between calculated and measured horizontal displacement at depths greater than 5.8 m is good. At 3.75 years, the calculated lateral displacement at the toe of the embankment is comparable to the measured lateral displacements. The calculated displacements agree with measured displacements up to 4 m below the original ground surface. The measured displacements exceed calculated displacements at depths greater than 4 m. In general, the agreement between the calculated and measured horizontal displacement profile at the embankment toe is considered to be acceptable.

Zones of soil at yield

Figure 14 shows the zones of normally consolidated (yielded) soil 13 years after the end of construction. At this time, the zones of yielded soil include much of the foundation layer directly beneath the test embankment between 1.2 and 5.2 m below the original ground level and a portion of the soil at a depth greater than 5.2 m. The yielding of the lower zones at a depth greater than 5.2 m is consistent with the findings of Lo et al. (1976), and Fig. 14 indicates that the calculated behaviour of the Gloucester test embankment is dominated by yielding of the upper 5.2 m of the foundation soil.

Stage 2: Gloucester test embankment

Centreline settlements

The geometry of stage 2 of the Gloucester test embankment is shown in Fig. 8. Construction of stage 2 was simulated over the course of 5 days in accordance with the construction records (supplied by NRC). The prediction of field settlements for stage 2 is complicated by the bilinear consolidation characteristic of the Gloucester foundation soil in the normally consolidated stress range and the lack of raw consolidation data for the case history. The consolidation data published by Leroueil et al. (1983) indicate that the transition phase of the consolidation curve (see Fig. 2) occurs over a stress range of approximately 25–30 kPa. To approximate the increased stiffness in the restructured range of the consolidation behaviour, the compression index, λ , in the restructured range was taken to be one half of the compression index in the transitional phase based on the consolidation curves published by Leroueil et al. (1983).

Figure 15 shows the comparison of calculated settlements with measured settlements beneath the embankment centreline for stage 2. The calculated settlement at the surface for a transitional stress range of 30 kPa is 41.5 cm compared with the measured settlement of approximately 36.0 cm. This represents a relative error of approximately 13% for the surface settlements during stage 2; however, including the deformations recorded during stage 1 of the case history, the relative error between measured and calculated settlements at centreline is approximately 7%. The calculated settlements up to 1 year after the end of construction are very close to the measured settlements. The calculated settlements exceed the measured settlements for times greater than 1 year. The rates of settlement are close to the measured rates of settlement during the first year after construction; however, 4 years after the end of construction, the rates of settlement and the compressive strains in the upper 1.45 m of the deposit are slightly overestimated at gauge S1.

Also shown in Fig. 15 are the calculated centreline settlements assuming a transitional stress range of 25 kPa. The settlements at the surface decrease to 39 cm for a transitional stress range of 25 kPa compared with 41.5 cm for a transitional stress range of 30 kPa and the measured centreline settlement of 36 cm. At a depth of 1.45 m, the calculated settlements are essentially the same regardless of the assumed transitional stress range, and the calculated compressive strains in the upper 1.45 m of the soil deposit are closer to the measured compressive strains. The relative

Fig. 14. Zones of yielded soil 13 years after the end of construction for stage 1 of the Gloucester test embankment.

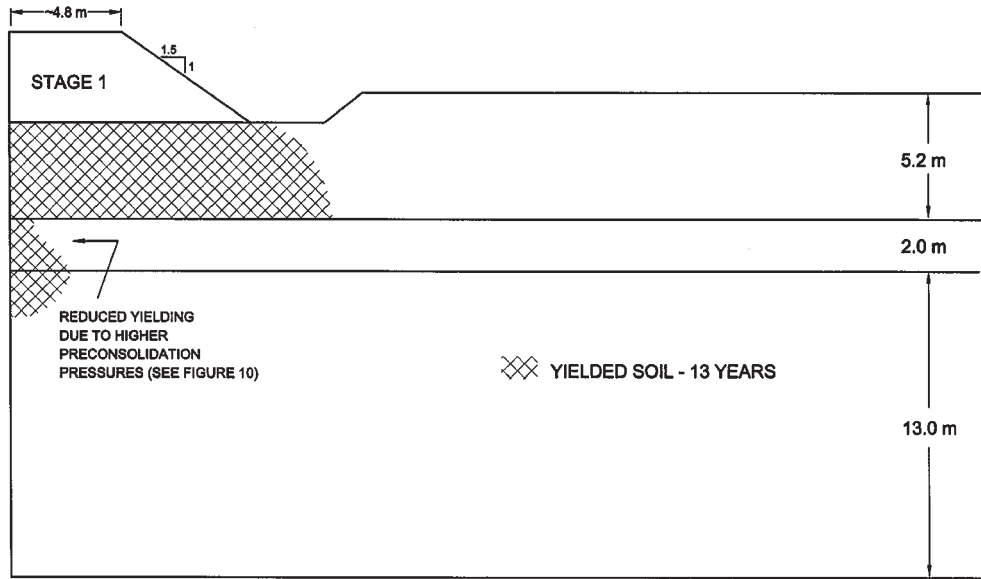
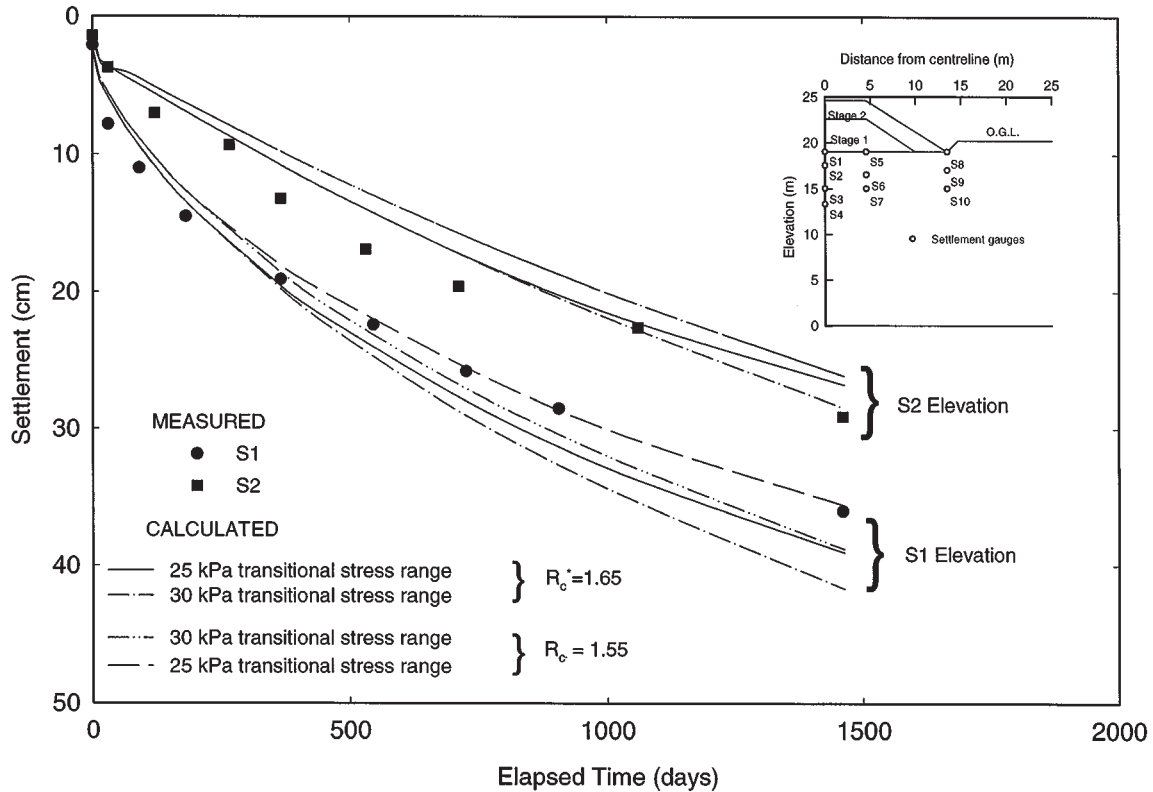


Fig. 15. Vertical deformations beneath centreline for stage 2 of the Gloucester test embankment. S1 and S2, settlement gauges; R_c^* , yield surface aspect ratio.

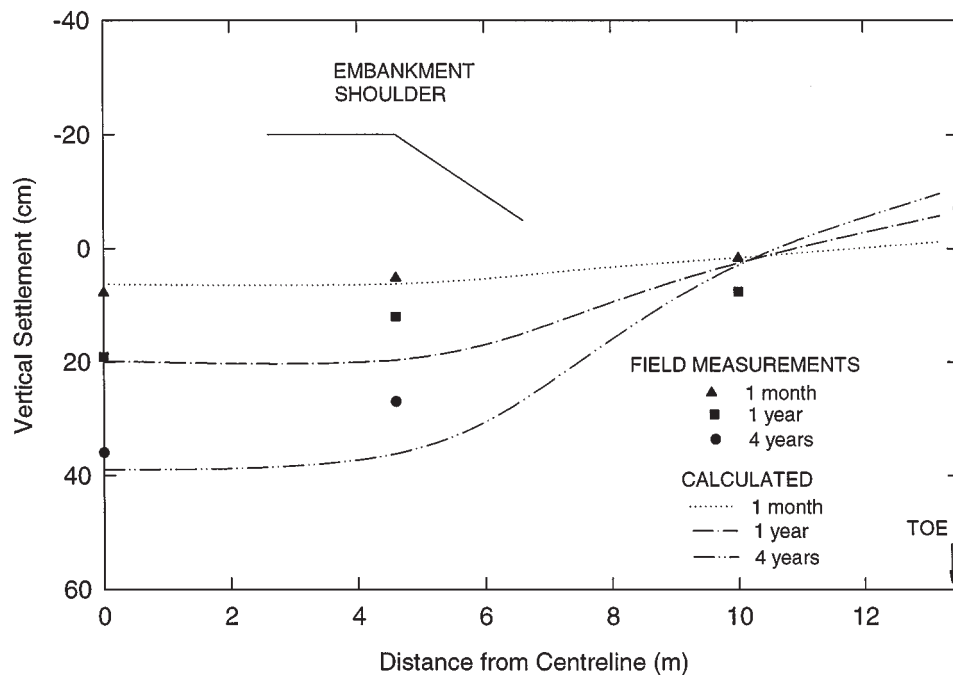


error between calculated and measured settlement 4 years after the end of construction of stage 2 is approximately 8%. The calculated rates of settlement for a transitional stress range of 25 kPa are in good agreement with the measured rate of settlement for settlement gauges S1 and S2 beneath the embankment centreline.

The aspect ratio, R_c , of 1.65 used above was selected based on two CIU compression tests at a depth of 2.4 m and

may not be representative of the entire soil deposit. To evaluate the influence of the yield-surface aspect ratio, R_c , on the calculated settlements, analyses were also performed assuming $R_c = 1.55$ for stages 1 and 2 and transitional stress ranges of 25 and 30 kPa, respectively. Figure 15 shows that the centreline settlements decrease with decreasing aspect ratio, R_c . For a transitional stress range of 25 kPa, the calculated settlement at centreline at 4 years is 35 cm for $R_c =$

Fig. 16. Comparison of calculated and measured surface settlement profile 1 month, 1 year, and 4 years after the end of construction for stage 2 of the Gloucester test embankment.



1.55 compared with 39 cm for $R_c = 1.65$. For a transitional stress range of 30 kPa, the calculated settlement at centreline at 4 years was 38.5 cm for $R_c = 1.55$ and 41 cm for $R_c = 1.65$. The measured settlement at 4 years (after the end of construction) was 36 cm.

In general, the elliptical cap elastoviscoplastic constitutive model is able to describe the settlement behaviour of stages 1 and 2 of the Gloucester test embankment for an aspect ratio, R_c , of 1.65 and transitional ranges of 25 and 30 kPa. The aspect ratio of the elliptical yield surface had only a small effect on the calculated settlement at centreline for the cases studied. The best agreement between calculated and measured behaviour was obtained for an aspect ratio, R_c , of 1.55 and a transitional stress range of 25 kPa; however, all calculated centreline settlements are adequate when compared with the field measurements. The transitional stress range has only a small effect on the settlement recorded at gauge S2 and improved the agreement between calculated and measured compression in the upper 1.45 m of the deposit.

Surface-settlement profile

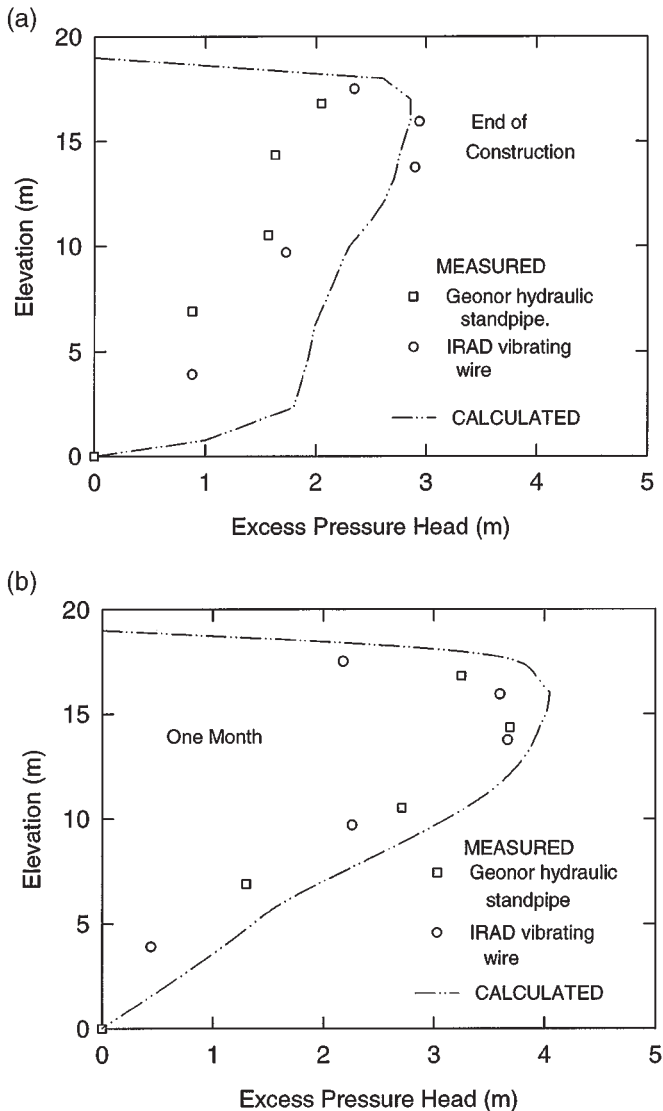
The calculated surface-settlement profiles corresponding to $R_c = 1.65$ and a transitional stress range of 25 kPa are shown in Fig. 16. The calculated surface settlements are generally in agreement with the measured surface settlement profiles 1 month, 1 year, and 4 years after the end of construction; however, the settlements beneath the embankment crest are overestimated at 1 year and 4 years. Given the uncertainties associated with modelling stage 2 of the Gloucester test embankment, the calculated settlement behaviour of stage 2 of the Gloucester test embankment is considered to be good.

Excess pore pressures

Figure 17 shows the comparison of calculated and measured excess pore pressures at the end of construction and 1 month after the end of construction. The background groundwater pressures at the site of the Gloucester test embankment were monitored during stage 2 with a series of piezometers installed 35 m from the location of the test embankment. This series of piezometers indicated that the background pore-pressure distribution remained relatively constant during the 4 year period after the end of construction. At the end of construction, the calculated excess pore pressures are in good agreement with the IRAD vibrating wire measurements and exceed the Geonor hydraulic standpipe measurements in the upper 5.2 m of the foundation. In the lower portion of the soil deposit the calculated pore pressures exceed both the hydraulic standpipe and vibrating wire measurements. The hydraulic standpipe piezometers appear to suffer from lag, as the measurements are lower than the vibrating wire measurements at all depths immediately after the end of construction and are in good agreement with the vibrating wire measurements 1 month after the end of construction.

One month after the end of construction the calculated excess pore pressures agree with both the hydraulic and vibrating-wire measurements at all depths. Comparing the excess pore pressures at the end of construction and 1 month after the end of construction shows an increase in the measured excess pore pressures during this time. The field measurements show a maximum increase of approximately 0.8 m from the end of construction to 1 month after the end of construction. The case records indicate that maximum recorded pore pressures beneath the embankment centreline

Fig. 17. Comparison of calculated and measured excess pore pressures (a) immediately after construction, and (b) 1 month after the end of construction.



occurred in most cases approximately 1 month after the end of construction. The calculated excess pore pressures increase by approximately 1 m from the end of construction to 1 month after the end of construction. Furthermore, the calculated maximum excess pore pressures occurred approximately 1 month after the end of construction.

Hydrodynamic lag cannot account for the magnitude of pore-pressure increases that occurred during this time period. Rather, the majority of the increased pore pressures during the initial undrained behaviour of the test embankment result from time-dependent plasticity. Figure 18 shows contours of overstress within the yield zone at the end of construction. This overstress represents the potential for plastic strain to occur due to the construction of stage 2 of the Gloucester test embankment. Excess pore pressures are induced as time-dependent plastic deformations occur and the stress states relax toward the field (static) yield surface.

Fig. 18. Contours of overstress at the end of construction of stage 2 of the Gloucester test embankment. O.G.L., original ground level.

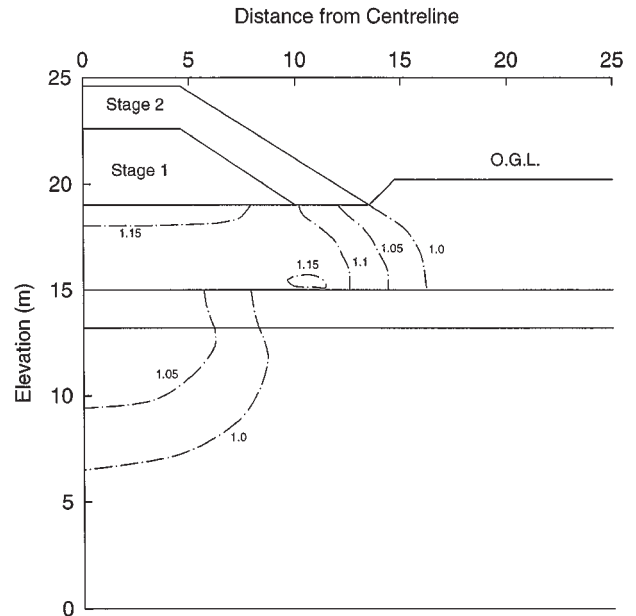


Figure 19 shows the calculated and measured excess pore pressure heads 1 year and 4 years after the end of construction of stage 2. The calculated excess pore pressures exceed the measured excess pore pressures at all depths. The dissipation of excess pore pressures between 1 year and 4 years is closely predicted by the method of analysis, and the computed distribution of excess pore pressures agrees with the hydraulic standpipe measurements 4 years after the end of construction of stage 2. The IRAD vibrating wire pressure heads are considerably lower than the more reliable hydraulic standpipe measurements 4 years after the end of construction.

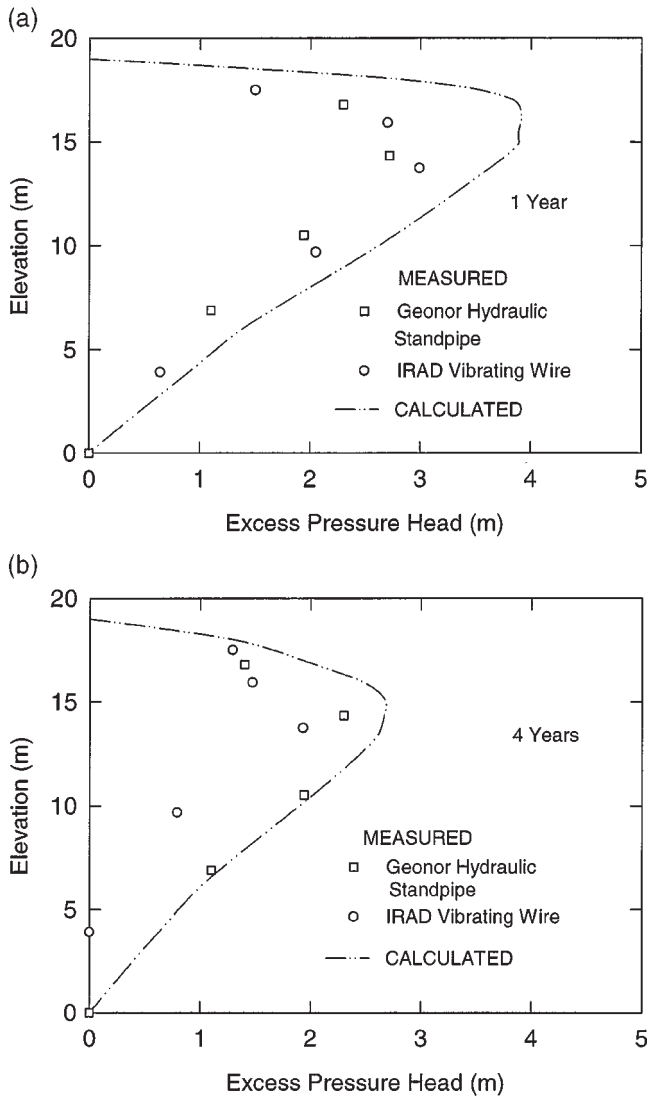
Lateral displacements

The comparison of measured and calculated horizontal displacements at the embankment toe and shoulder 1 month after the end of construction are shown in Fig. 20. The calculated lateral displacements exceed the measured horizontal displacements beneath both the embankment shoulder and the toe. This trend was also observed at the end of construction, 1 year and 4 years after the end of construction. In general, 1 month after the end of construction both measured and calculated horizontal displacements are small.

Discussion

The ability of the elastoviscoplastic constitutive model used in this paper to describe the secondary compression behaviour of the Gloucester foundation soil during long-term Rowe cell consolidation tests has been demonstrated. An elliptical cap with an aspect ratio, R_c , of 1.65 could also adequately describe the behaviour of the Gloucester foundation soil during CIU triaxial tests. Since the consolidation stage of the CIU triaxial tests exceeded the preconsolidation pressure of the Gloucester soil, the Rowe cell consolidation be-

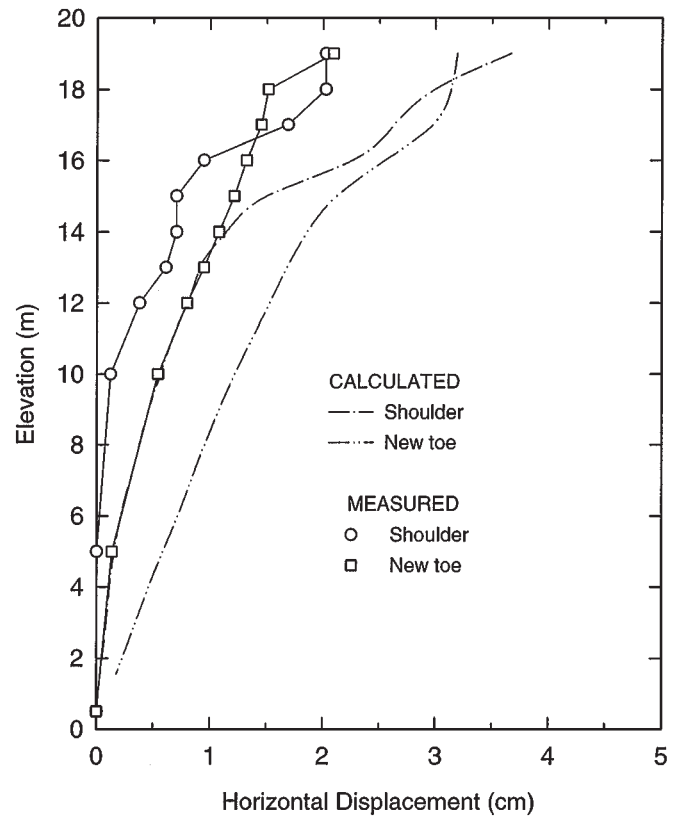
Fig. 19. Comparison of measured and calculated excess pore pressures (a) 1 year and (b) 4 years after the end of construction.



behaviour and CIU triaxial test behaviour correspond to the restructured or residual soil fabric. The viscosity constants calculated from the results of long-term Rowe cell consolidation tests were used to consider the effect of strain rate and duration of consolidation during the CIU triaxial tests using the elliptical cap model. The aspect ratio of the elliptical cap was selected so that the calculated behaviour during CIU triaxial compression tests matched the measured behaviour. Also, the theoretical long-term shear strength for an elliptical cap with $R_c = 1.65$ was found to be comparable to the undrained shear strength during UU triaxial tests conducted at very slow strain rates.

A number of researchers have investigated the in situ and laboratory yielding of cohesive soils (see Mitchell 1970; Tavenas and Leroueil 1977; Lew 1981; Folkes and Crooks 1985). In general, the existence of a yield surface for cohesive soils is accepted; however, the available literature indicates that the measured or apparent shape of the yield surface varies from soil to soil. The elliptical cap yield sur-

Fig. 20. Comparison of calculated and measured horizontal displacements for stage 2, 1 month after the end of construction.



face was adopted for the analysis presented in this paper, since the aspect ratio, R_c , can be used to vary the yield-surface shape. The present study has extended the calibration process described by Chen (1982) for elliptical yield surfaces to include the effect of time-dependent plastic deformations. The viscoplastic constants used in this paper correspond to the residual or restructured soil fabric and can adequately describe the strain-rate-dependent behaviour of the residual shear strength during UU triaxial tests as well as the behaviour during CIU triaxial tests at consolidation stresses that exceed the preconsolidation pressure of the Gloucester foundation soils.

The elliptical cap model with $R_c = 1.65$ and other parameters based on laboratory data were successfully used to predict the behaviour of two stages of construction (stage 1 in 1967 and stage 2 in 1982) of the Gloucester test embankment, generally giving good agreement between the calculated and measured settlements. During stage 1, the calculated horizontal displacements at the toe of the test embankment are in agreement with the measured horizontal displacements. The field measurements indicated that stage 2 of the test embankment performed slightly better than calculated. For stage 2 of the Gloucester test embankment, the method of analysis closely described the surface-settlement profiles, centreline settlements, and the excess pore pressure response beneath the embankment centreline and embankment toe. Settlements beneath the embankment crest and excess pore pressures beneath the embankment crest were consistently overestimated.

It should be noted that the impact of stage 1 settlements on the embankment geometry prior to stage 2 was not considered (e.g., small strain analysis). Furthermore, the case records (NRC) indicate that the embankment crest was graded to provide drainage. It may be that the fill thickness at the crest is less than the fill thickness at centreline as a result of the stage 1 settlements and grading of the embankment to provide drainage. Differences between the assumed embankment geometry and actual embankment geometry may account for some of the difference between calculated and measured behaviour. Uncertainty associated with the stress state within the embankment fill just prior to stage 2 and the embankment loads transferred to the foundation may also account for a significant portion of the difference between calculated and measured behaviour. In addition to uncertainties associated with the embankment geometry and embankment loads, anisotropy of the Gloucester foundation soil may have had an impact on the embankment performance and may also account for some of the difference between calculated and measured behaviour. In particular, the agreement between calculated and measured horizontal displacements during stage 2 is limited (see Fig. 20). Given the better agreement between the calculated and measured horizontal displacements for stage 1 (see Fig. 13), some anisotropy may have been induced during consolidation under stage 1 loads. This induced anisotropy may contribute to some of the observed difference between calculated and measured horizontal displacements during stage 2. Given the uncertainties associated with predicting embankment performance, however, the agreement between calculated and measured behaviour is encouraging and the test embankment performed marginally better than calculated.

The results of this study indicate that the behaviour of the Gloucester foundation soil during laboratory and field tests can be described using a single elastoviscoplastic yield-surface model. Evidence of the presence of a field preconsolidation pressure (yield surface) which is less than the measured preconsolidation pressure has been presented, providing additional support for the concepts proposed by Bjerrum (1967). Based on the available data, it would appear that the Gloucester foundation soil exhibits a strain-softening response only during UU triaxial compression tests for axial strain rates in excess of approximately 0.001%/min. At axial strain rates lower than 0.001%/min, the Gloucester foundation soil behaved as a strain-hardening material (Law 1974). Leroueil et al. (1983) estimated that the in situ compressive strain rate within the foundation soils for stage 1 of the Gloucester test embankment was 2.0×10^{-5} %/min at the end of construction and 2.0×10^{-6} %/min at 1.5 years after the end of construction. As a result it was assumed that the strain-hardening behaviour was operative in the field and that the Gloucester foundation soil tends toward the residual or restructured state in the field. Considering the good agreement between calculated and measured behaviour, this assumption appears to be supported by the present analysis.

Conclusions

Based on the results presented in this paper, the following conclusions are made:

(1) Much of the behaviour of the Gloucester foundation soil during laboratory and field loading conditions can be adequately described using yield-surface concepts and over-stress viscoplasticity.

(2) An elliptical yield surface with an aspect ratio of about $R_c = 1.65$ appears to be representative of the field yield surface of the Gloucester foundation soil.

(3) Both experimental and analytical evidence has been presented to show that the aspect ratio of the field yield surface can be estimated from conventional laboratory tests provided that due consideration is given to strain-rate effects. It may be possible to infer the yield-surface aspect ratio from a standard incremental oedometer consolidation test and triaxial compression test at similar strain rates. This approach, however, warrants further study.

(4) The in situ field preconsolidation pressure of the Gloucester foundation soil may be slightly overestimated using conventional laboratory tests, since the strain rates are higher than those expected in the field.

(5) The increase in excess pore pressures during the initial month after the end of construction of stage 2 of the Gloucester test embankment can be explained and is described well by time-dependent plasticity and yield-surface theory.

Acknowledgement

The research reported in this paper was funded by a research grant from the Natural Sciences and Engineering Research Council of Canada.

References

- Adachi, T., and Oka, F. 1982. Constitutive equations for normally consolidated clay based on elasto-viscoplasticity. *Soils and Foundations*, **22**(4): 57–70.
- Adachi, T., and Okano, M. 1974. A constitutive equation for normally consolidated clay. *Soils and Foundations*, **14**: 55–73.
- Bjerrum, L. 1967. Engineering geology of Norwegian normally-consolidated marine clays as related to settlements of buildings. *Géotechnique*, **17**: 81–118.
- Booker, J.R., and Small, J.C. 1975. An investigation of the stability of numerical solutions of Biot's equations of consolidation. *International Journal of Solids and Structures*, **11**: 907–911.
- Bozozuk, M. 1974. Minor principal stress measurements in marine clay with hydraulic fracture tests. *In Proceedings, ASCE Engineering Foundation Special Conference on Subsurface Exploration for Underground Excavations and Heavy Construction, New England College, Henniker, N.H., August 11–16*, pp. 333–349.
- Bozozuk, M., and Leonards, G.A. 1972. The Gloucester test fill. *In Proceedings, ASCE Special Conference on Performance of Earth and Earth-Supported Structures, Purdue University, Lafayette, Ind., Vol. 1, Part 1*, pp. 299–317.
- Britto, A.M., and Gunn, M.J. 1987. Critical state soil mechanics via finite elements. Ellis Horwood, Chichester, England.
- Carter, J.P., and Balaam, N.P. 1990. AFENA — A general finite-element algorithm: users manual. School of Civil Engineering and Mining Engineering, University of Sydney, Sydney, NSW, Australia.
- Chen, W.F. 1982. *Plasticity in reinforced concrete*. McGraw-Hill, New York.

- Cormeau, I. 1975. Numerical stability of quasi-static elasto/viscoplasticity. *International Journal of Numerical Methods in Engineering*, **9**: 109–127.
- Davis, E.H. 1968. Theories of plasticity and failure of soil masses. *In Soil mechanics — selected topics. Edited by I.K. Lee.* Butterworths, London, Chap. 6.
- Desai, C.S., and Zhang, D. 1987. Viscoplastic model for geological materials with generalized flow rule. *International Journal for Numerical and Analytical Methods in Geomechanics*, **11**: 603–620.
- Fisher, D.G., Rowe, R.K., and Lo, K.Y. 1982. Prediction of the second stage behaviour of Gloucester Test Fill. The University of Western Ontario, Geotechnical Research Report GEOT-4-82.
- Folkes, D.J., and Crooks, J.H.A. 1985. Effective stress paths and yielding in soft clays below embankments. *Canadian Geotechnical Journal*, **22**: 357–374.
- Gibson, R.E., and Lo, K.Y. 1961. A theory of consolidation of soils exhibiting secondary consolidation. Norges Geotekniske Institut Publication No. 41.
- Hinchberger, S.D. 1996. The behaviour of reinforced and unreinforced embankments on soft rate sensitive foundation soils. Ph.D. thesis, The University of Western Ontario, London, Ont.
- Janbu, N. 1963. Soil compressibility as determined by oedometer and triaxial tests. *In Proceedings of the European Conference on Soil Mechanics and Foundation Engineering*, Wiesbaden, Germany, Vol. 1, pp. 19–25.
- Katona, M.G. 1984. Evaluation of viscoplastic cap model. *Journal of Geotechnical Engineering*, ASCE, **110**(8): 1106–1125.
- Kavazanjian, E., Jr., Borja, R.I., and Jong, H.L. 1985. Time-dependent deformations in clay soils. *In Proceedings of the 11th International Conference on Soil Mechanics and Foundation Engineering*, San Francisco, Rotterdam, pp. 11–16.
- Law, K.T. 1974. Analysis of embankments on sensitive clays. Ph.D. thesis, The University of Western Ontario, London, Ont.
- Leroueil, S., Sampson, L., and Bozozuk, M. 1983. Laboratory and field determination of preconsolidation pressures at Gloucester. *Canadian Geotechnical Journal*, **20**: 477–490.
- Lew, K.V. 1981. Yielding criteria and limit state in a Winnipeg clay. M.Sc. thesis, University of Manitoba, Winnipeg.
- Lo, K.Y., and Morin, J.P. 1972. Strength anisotropy and time effects of two sensitive clays. *Canadian Geotechnical Journal*, **9**(3): 261–277.
- Lo, K.Y., Bozozuk, M., and Law, K.T. 1976. Settlement analysis of the Gloucester test fill. *Canadian Geotechnical Journal*, **13**(4): 339–354.
- Massachusetts Institute of Technology. 1975. Proceedings of the Foundation Deformation Prediction Symposium. U.S. Department of Transportation, Report FHWA-RD-75-515, Vols. 1 and 2.
- McCarron, W.O., and Chen, W.F. 1987. A capped plasticity model applied to Boston blue clay. *Canadian Geotechnical Journal*, **24**: 630–644.
- Mesri, G., and Choi, Y.K. 1979. Excess pore water pressure during consolidation. *In Proceedings of the 6th Asian Regional Conference on Soil Mechanics and Foundation Engineering*, Singapore, Vol. 1, pp. 151–154.
- Mitchell, R.J. 1970. On the yielding and mechanical strength of Leda clays. *Canadian Geotechnical Journal*, **7**: 297–312.
- Norton, F.H. 1929. Creep of steel at high temperatures. McGraw-Hill Book Co., New York.
- Oka, F., Adachi, T., and Okano, Y. 1986. Two dimensional consolidation analysis using an elasto-viscoplastic constitutive equation. *International Journal for Numerical and Analytical Methods in Geomechanics*, **10**: 1–16.
- Owen, D.R.J., and Hinton, E. 1980. Finite elements in plasticity: theory and practice. Pineridge Press, Swansea, England.
- Perzyna, P. 1963. The constitutive equations for work-hardening and rate sensitive plastic materials. *In Proceedings, Conference on Vibrational Problems*, Warsaw, Vol. 4, No. 3, pp. 281–290.
- Redman, P., and Poulos, H. 1984. Study of two field cases involving undrained creep. *Journal of Geotechnical Engineering*, ASCE, **110**(9): 1307–1321.
- Roscoe, K.H., and Burland, J.B. 1968. On the generalized stress-strain behaviour of “wet” clay. *In Engineering plasticity. Edited by J. Heyman and F. Leeckie.* Cambridge University Press, Cambridge, England, pp. 535–609.
- Roscoe, K.H., and Schofield, A.N. 1963. Mechanical behaviour of an idealised “wet clay.” *In Proceedings of the 2nd European Conference on Soil Mechanics*, Wiesbaden, Vol. 1, pp. 47–54.
- Rowe, R.K., and Hinchberger, S.D. 1998. The significance of rate effects in modelling the Sackville test embankment. *Canadian Geotechnical Journal*, **35**: 500–516.
- Rowe, R.K., McLean, M.D., and Soderman, K.L. 1984. Analysis of a geotextile reinforced embankment constructed on peat. *Canadian Geotechnical Journal*, **21**(3): 563–576.
- Rowe, R.K., Gnanendran, C.T., Landva, A.O., and Valsangkar, A.J. 1996. Calculated and observed behaviour of a reinforced embankment over soft compressible soil. *Canadian Geotechnical Journal*, **33**(2): 324–338.
- Silvestri, V. 1984a. Preconsolidation pressure of Champlain clays. Part II. Laboratory determination: Discussion. *Canadian Geotechnical Journal*, **21**: 600–602.
- Silvestri, V. 1984b. Laboratory and field determination of preconsolidation pressures at Gloucester: Discussion. *Canadian Geotechnical Journal*, **21**: 602–603.
- Tavenas, F., and Leroueil, S. 1977. Effects of stresses and time on yielding of clays. *In Proceedings of 9th International Conference on Soil Mechanics and Foundation Engineering*, Tokyo, Vol. 1, pp. 319–326.
- Zienkiewicz, O.C., and Cormeau, I.C. 1974. Visco-plasticity – plasticity and creep in elastic solids — a unified numerical solution approach. *International Journal for Numerical Methods in Engineering*, **8**: 821–845.

Appendix

The basic elastoviscoplastic formulation adopted in this paper is summarized below. Full details are given by Hinchberger (1996). The strain-rate tensor for an elastoviscoplastic material is expressed as

$$[A1] \quad \dot{\epsilon}_{ij} = \dot{\epsilon}_{ij}^e + \dot{\epsilon}_{ij}^{vp}$$

where $\dot{\epsilon}_{ij}^e$ and $\dot{\epsilon}_{ij}^{vp}$ are the elastic and viscoplastic strain-rate tensors, respectively. For stress states below yield, the elastic bulk modulus, K , was considered to be stress dependent and given by

$$[A2] \quad K = (1 + e) \frac{\sigma'_m}{\kappa}$$

where κ is the recompression index, e is the void ratio, and $\sigma'_m = (\sigma_1 + \sigma_2 + \sigma_3)/3$ is the mean effective stress. The shear modulus, G , is related to the bulk modulus, K , through eq. [A3]:

$$[A3] \quad G = \frac{3(1 - 2\nu)K}{2(1 + \nu)}$$

where ν is Poisson's ratio and was assumed to remain constant. The viscoplastic strain-rate tensor is expressed as

$$[A4] \quad \dot{\epsilon}_{ij}^{vp} = \gamma^{vp} \langle \Phi(F) \rangle \frac{\partial f}{\partial \sigma'_{ij}}$$

where γ^{vp} is the viscoplastic fluidity parameter with units of inverse time, the scalar function $\Phi(F)$ is called the flow function, and $\partial f / \partial \sigma'_{ij}$ is the derivative of the plastic potential for associated viscoplasticity. The elliptical cap yield function (Chen 1982) was used to define yielding in the normally consolidated stress range, and the equation of the elliptical cap in $(2J_2)^{1/2} - \sigma'_m$ stress space is

$$[A5] \quad f^{(s)} = (\sigma'_m - l)^2 + 2J_2(R_c^2) - (\sigma_{my}^{(s)} - l)^2 = 0$$

where l is the σ'_m coordinate of the centre of the ellipse, is the yield-surface intercept with the σ'_m axis, J_2 is the second invariant of the deviatoric stress tensor, and σ'_m is the mean effective stress. The geometry of the elliptical yield surface is shown in Fig. 1. The elastoviscoplastic constitutive equation associated with the elliptical cap yield surface in the normally consolidated stress range is

$$[A6] \quad \dot{\epsilon}_{ij} = \frac{\dot{s}_{ij}}{2G} + \frac{\kappa}{3(1+e)} \frac{\dot{\sigma}'_m}{\sigma'_m} \delta_{ij} + \gamma^{vp} \langle \Phi(F) \rangle \left[\frac{\delta_{ij}}{3} - \left(\frac{2l}{\sigma_{my}^{(d)}} - 1 \right) \left(\frac{\sigma_{my}^{(d)}}{\sigma'_m} \right)^2 \frac{\delta_{ij}}{3} - R_c^2 \left(\frac{\sqrt{2J_2}}{\sigma'_m} \right)^2 \frac{\delta_{ij}}{3} + \frac{2s_{ij}R_c^2}{\sigma'_m} \right]$$

$$\Phi(F) = \left(\frac{\sigma_{my}^{(s)} + \sigma_{os}^{(d)}}{\sigma_{my}^{(s)}} \right)^n$$

where s_{ij} is the deviatoric stress tensor, G is the shear modulus, κ is the recompression index, e is the void ratio, δ_{ij} is Kronecker's delta, γ^{vp} is the viscoplastic fluidity constant, n is the strain-rate exponent, $\sigma_{my}^{(s)}$ is the static yield-surface intercept, $\sigma_{my}^{(d)}$ is the dynamic yield-surface intercept, σ'_m is the mean effective stress, R_c is the yield-surface aspect ratio in $(2J_2)^{1/2} - \sigma'_m$ stress space, $\Phi(F)$ is the viscoplastic flow function, and $\sigma_{os}^{(d)}$ is the overstress (see Fig. 1).

For yielding in the normally consolidated stress range, overstress, $\sigma_{os}^{(d)}$, was calculated as the orthogonal distance between parallel yield-surface tangents in $(2J_2)^{1/2} - \sigma'_m$ stress space. At failure, the overstress, $\sigma_{os}^{(d)}$, was a function of the second invariant of the deviatoric stress tensor J_2 . The expansion of the yield surface is a time-dependent process depending on the current viscoplastic increment of volumetric strain, $\partial \epsilon_{vol}^{vp}$, as governed by

$$[A7] \quad \partial \sigma_{my}^{(s)} = \frac{(1+e)}{\lambda - \kappa} \sigma_{my}^{(s)} \partial \epsilon_{vol}^{vp}$$

Failure in both the normally consolidated and overconsolidated stress ranges has been defined using a Drucker-Prager failure envelope:

$$[A8] \quad f^{(s)} = M\sigma'_m + c'_k - \sqrt{2J_2} = 0$$

where M is the slope of the failure envelope in $(2J_2)^{1/2} - \sigma'_m$ stress space, c'_k is the cohesion intercept, σ'_m is the mean effective stress, and J_2 is the second invariant of the deviatoric stress tensor.

Viscoplastic stress and strain increments

The viscoplastic strain-rate vector, $\{\dot{\epsilon}^{vp}\}$, at time step $m + 1$ can be obtained using Taylor series and ignoring higher order terms:

$$[A9] \quad \{\dot{\epsilon}^{vp}\}_{m+1} = \{\dot{\epsilon}^{vp}\}_m + \left[\frac{\partial \dot{\epsilon}^{vp}}{\partial \sigma} \right]_m \{\Delta \sigma\}_m = \{\dot{\epsilon}^{vp}\}_m + [H]_m \{\Delta \sigma\}_m$$

where $\{\Delta \sigma\}_m$ is the vector of stress increment, and $[H]_m$ denotes the gradient of the viscoplastic strain-rate vector with respect to effective stress at time m . The viscoplastic strain increment $\{\Delta \epsilon^{vp}\}$ during the time interval $\Delta t_m = t_{m+1} - t_m$ can be written as follows:

$$[A10] \quad \{\Delta \epsilon^{vp}\}_m = \Delta t_m [(1 - \theta)\{\dot{\epsilon}^{vp}\}_m + \theta\{\dot{\epsilon}^{vp}\}_{m+1}]$$

where θ is a numerical constant. For $\theta = 0$, the simple Euler scheme is obtained (Zienkiewicz and Corneau 1974). For the analyses presented in this paper, an incremental approach to the solution of elastoviscoplastic continuum problems was adopted using $\theta = 0.5$ with small time step increment sizes. The time step requirements for stability published by Corneau (1975) and Owen and Hinton (1980) were found to be helpful guidelines for stability of the solutions obtained.

The stress increment vector, $\{\Delta \sigma\}_m$, can be written as follows:

$$[A11] \quad \{\Delta \sigma\}_m = [C^e]\{\Delta \epsilon\}_m = [C^e](\{\Delta \epsilon\}_m - \{\Delta \epsilon^{vp}\}_m)$$

where $\{\Delta \epsilon\}_m = [B]_m\{\Delta a\}$, $[B]$ is the strain-displacement transformation matrix, and $\{\Delta a\}$ is the incremental vector of nodal displacements. Substitution of eq. [A10] into eq. [A11] gives

$$[A12] \quad \{\Delta \sigma\}_m = \left[[I] + [C^e](\theta \Delta t_m [H]_m) \right]^{-1} [C^e]([B]_m\{\Delta a\}_m - \{\dot{\epsilon}^{vp}\}_m \Delta t_m)$$

where $[I]$ is the identity matrix, $[C^e]$ is the elastic constitutive matrix, θ is a numerical constant (0.5), Δt_m is the current time increment, $[H]_m$ is the derivative of the viscoplastic strain-rate vector with respect to stress, $[B]_m$ is the strain-displacement transformation matrix, $\{\Delta a\}$ is the vector of nodal displacements, and $\{\dot{\epsilon}^{vp}\}_m$ is the current viscoplastic strain-rate vector.

Coupled finite-element equations

Applying the principle of virtual work to the equilibrium equation and dropping the incremental subscript, m , gives the following relationship for the load increment:

$$[A13] \quad \int_V \{\delta \epsilon\}^T \{\Delta \sigma\} dV = \int_V \{\delta \epsilon\}^T \{\Delta \sigma'\} dV + \int_V \{\delta \epsilon\}^T \{\Delta u_w\} dV \\ = \int_V \{\delta d\}^T \{\Delta F_b\} dV + \int_s \{\delta d\}^T \{\Delta T\} ds$$

where $\{\delta \epsilon\}$ is the incremental strain vector, $\{\Delta \sigma\}$ is the incremental total stress vector, $\{\Delta \sigma'\}$ is the incremental effective stress vector, $\{\Delta u_w\}$ is the incremental pore-water pressure vector, $\{\delta d\}$ is the vector of incremental displacements, $\{\Delta F_b\}$ is the incremental body force vector, and $\{\Delta T\}$ is the applied surface load incremental vector. Within a typical element, the variation of incremental displacement is

$$[A14] \quad \{\delta d\} = [N] \{\delta a\}$$

where $[N]$ is the matrix of shape functions, and $\{\delta a\}$ is the incremental nodal displacement vector. Applying the same shape functions, $[N]$, the variation of excess pore-water pressures within a typical element are

$$[A15] \quad \{\Delta u_w\} = [N] \{\Delta b\}$$

where $\{\delta b\}$ are the incremental nodal values of excess pore pressure. The strain increment vector, $\{\Delta \epsilon\}$, and the incremental volumetric strain vector, $\{\Delta v\}$, within a typical element are given by

$$[A16] \quad \{\Delta \epsilon\} = [B] \{\Delta a\}$$

and

$$[A17] \quad \{\Delta v\} = \{m\}^T \{\Delta \epsilon\} = \{m\}^T [B] \{\Delta a\}$$

where $[B]$ is the strain-nodal displacement transformation matrix, and $\{m\}$ is defined as follows:

$$[A18] \quad \{m\} = \begin{bmatrix} 1 \\ 1 \\ 1 \\ 0 \end{bmatrix}$$

Substituting eqs. [A14]–[A17] into eq. [A13] results in the following finite-element equations:

$$[A19] \quad [k^e] \{\Delta a\} + [L] \{\Delta b\} = \{\Delta F\}$$

where

$$[A20] \quad [K^e] = \int_V [B]^T [C^e] [B] dV$$

$$[A21] \quad [L] = \int_V [B]^T \{m\} [N] dV$$

$$[A22] \quad \{\Delta F\} = \int_V [N]^T \{\Delta F_b\} dV \\ + \int_s [N]^T \{\Delta T\} ds + \int_V \{\Delta \sigma_R\} dV$$

In eq. [A22], $\{\Delta \sigma_R\}$ is the vector of viscoplastic relaxation stresses defined by

$$[A23] \quad \{\Delta \sigma_R\} = [B]^T [\bar{C}] \{\dot{\epsilon}^{vp}\} \Delta t$$

and

$$[A24] \quad [\bar{C}] = [I + C^e(\theta \Delta t H)]^{-1} [C^e]$$

Applying a similar virtual work principle to the two-dimensional equation of continuity results in the following expression:

$$[A25] \quad \int_{\text{vol}} \{\delta b\} \left[\frac{k_{11}}{\gamma_w} \frac{\partial^2 u_w}{\partial x_{11}^2} + \frac{k_{33}}{\gamma_w} \frac{\partial^2 u_w}{\partial x_{33}^2} + \frac{\partial v}{\partial t} \right] d(\text{vol}) = 0$$

where k_{11} is the hydraulic conductivity in the one-coordinate direction, k_{33} is the hydraulic conductivity in the three-coordinate direction, γ_w is the unit weight of the pore water, v is the seepage velocity, and t is the time. The gradient of excess pore pressure is given by

$$[A26] \quad \begin{bmatrix} \frac{\partial u_w}{\partial x_{11}} \\ \frac{\partial u_w}{\partial x_{33}} \end{bmatrix} = [E] \{\Delta b\}$$

where the terms of the matrix $[E]$ are obtained by differentiating the shape functions $[N]$. Substituting eqs. [A14]–[A17] and [A26] into eq. [A25] and solving gives

$$[A27] \quad [L]^T \frac{d\{a\}}{dt} - \Phi_k \{b\} = \int_s [N]^T \{v_n\} dA$$

where

$$[A28] \quad L = \int_V [B]^T m [N] dv$$

$$[A29] \quad \Phi_k = \int_V \frac{[E]^T [k] [E]}{\gamma_w} dV$$

and v_n is the prescribed boundary seepage velocity, and $[k]$ is the hydraulic conductivity matrix

$$[A30] \quad [k] = \begin{bmatrix} k_{11} & 0 \\ 0 & k_{33} \end{bmatrix}$$

Equation [A27] is a first-order differential equation which may be integrated with respect to time to give

$$[A31] \quad [L]^T \{\Delta a\} - \Phi_k \left[(1 - \beta) \{b(t)\} + \beta \{b(t + \Delta t)\} \right] \\ = \int_s [N]^T \left((1 - \beta) \{v_n(t)\} + \beta \{v_n(t + \Delta t)\} \right) \Delta t dA$$

where the value of β is a numerical constant and defines the variation of excess pore pressure, b , during the time interval. Booker and Small (1975) have shown that for unconditional stability, $\beta \geq 0.5$. A value of $\beta = 1$ was adopted based on Britto and Gunn (1987), reducing eq. [A31] to

$$[A32] \quad [L]^T \{\Delta a\} - \Phi_k \Delta t \{\Delta b\} \\ = \Phi_k \Delta t \{b\} + \int_s [L]^T v_n(t + \Delta t) \Delta t dA = \{\Delta F_s\}$$

Equations [A19] and [A32] can be used to establish a solution at $t + \Delta t$ from the solution at time t . To summarize, the fully coupled finite-element equations can be written as

$$[A33] \begin{bmatrix} [K^e] & [L] \\ [L]^T & -\Phi_k \Delta t \end{bmatrix} \begin{bmatrix} \{\Delta a\} \\ \{\Delta b\} \end{bmatrix} = \begin{bmatrix} \{\Delta F\} \\ \{\Delta F_s\} \end{bmatrix}$$

The implementation of the coupled elastoviscoplastic constitutive behaviour presented above is similar to the coupled finite-element implementation described by Britto and Gunn (1987); however, $[K^e]$ is the elastic element stiffness matrix, and $\{\Delta F\}$ contains additional terms related to the integration of the viscoplastic relaxation stresses defined by eqs. [A23] and [A24].

Material properties

The material constants for the elastoviscoplastic constitutive model can be subdivided into three categories as follows: constants associated with conventional elastoplastic analysis (κ , λ , ν , R_c , M , $\sigma_{my}^{(s)}$, and e), hydraulic conductivity constants (k_h , k_v , e_o , and C_k), and viscoplastic constants (n and γ^{vp}). The estimation of conventional elastoplastic con-

stants and hydraulic conductivity constants has been described in the literature by McCarron and Chen (1984, 1987) and Britto and Gunn (1987) and will not be described here. For the present formulation, two additional material constants (the strain-rate exponent, n , and the fluidity parameter, γ^{vp}) have been introduced to describe the time-dependent plastic (viscoplastic) deformations. These viscoplastic material constants can be estimated by fitting long-term consolidation test results using trial-and-error procedures. The results of this fitting procedure have been presented in the present paper for the Gloucester foundation soil. Alternatively, eq. [2] can be used to fit the results of conventional undrained triaxial tests (e.g., UU or CIU) performed at different strain rates. This latter approach can be used to provide an estimate of the strain-rate exponent, n , and fluidity parameter, γ^{vp} , for use with the elastoplastic constitutive model described above. It is recommended, however, that long-term consolidation tests be used to verify and refine the material constants obtained using eq. [2].